NIH Public Access
Author Manuscript

TRIVALENT LIGANDS WITH RIGID DNA SPACERS REVEAL STRUCTURAL REQUIREMENTS FOR IgE RECEPTOR SIGNALING IN RBL MAST CELLS

Dwaipayan Sil[1], **Jong Bum Lee**[2], **Dan Luo**[2], **David Holowka**[1], and **Barbara Baird**[1],*

[1]Department of Chemistry and Chemical Biology Cornell University, Ithaca, NY 14853

[2]Department of Biological and Environmental Engineering Cornell University, Ithaca, NY 14853

Abstract

Antigen-mediated crosslinking of immunoglobulin E (IgE) bound to its receptor, FcεRI, stimulates degranulation, phospholipid metabolism, and cytokine production in mast cells and basophils to initiate inflammatory and allergic responses. Previous studies suggested that spatial organization of the clustered receptors affects the assembly of the transmembrane signaling complexes. To investigate systematically the structural constraints in signal initiation, we utilized rigid, double-stranded DNA scaffolds to synthesize ligands with tunable lengths. We characterized a series of symmetric trivalent DNA ligands with rigid spacing between 2,4-dinitrophenyl (DNP) haptenic groups in range of 5 − 15 nm. These ligands all bind to anti-DNP IgE on RBL mast cells with similar avidity, and they all crosslink IgE-FcεRI complexes effectively. We observe length dependent stimulation of tyrosine phosphorylation of FcεRI β and γ subunits and the adaptor protein LAT: the shortest ligand is ~5−10-fold more potent than the longest. Stimulated Ca^{2+} mobilization and degranulation also exhibits kinetics and magnitudes that differ as a function of ligand length. In contrast, tyrosine phosphorylation of phospholipase Cγ1 and consequent Ca^{2+} release from intracellular stores do not show this dependence on ligand length. Our results with these rigid, DNA-based ligands provide direct support for receptor transphosphorylation as a key step in amplified signaling leading to degranulation, and they further reveal branching of pathways in signaling events.

Keywords

receptor crosslinking; tyrosine phosphorylation; phospholipase Cγ activation; calcium mobilization; degranulation

INTRODUCTION

Crosslinking of IgE-FcεRI on mast cells by specific oligovalent antigen initiates activation of degranulation and other cellular responses leading to inflammation and allergies (1). Receptor clustering causes transmembrane coupling with Src family tyrosine kinase Lyn, which phosphorylates FcεRI β and γ subunits (2). This interaction occurs within ordered membrane domains (lipid rafts) that provide protection from excluded phosphatases (3).

Transphosphorylation FcεRI-β and -γ by Lyn associated with an adjacent FcεRI-β in a clustered complex has been proposed as a key amplification mechanism (4). Phosphorylated FcεRI-γ recruits tyrosine kinase Syk to be phosphorylated by Lyn (5). Thus activated, Syk phosphorylates a number of proteins, including the adaptor LAT that mediates interactions with lipases and other proteins (6). Among the lipases, phospholipase Cγ1 and Cγ2 (PLCγ1 and PLCγ2) are activated by tyrosine phosphorylation and hydrolyze phosphatidylinositol-4,5-bisphosphate (PIP$_2$) to generate inositol $-$1,4,5-triphosphate (IP$_3$), which initiates Ca^{2+} mobilization (7). These stimulated events lead to mast cell degranulation and release from secretory granules of histamine and other intercellular chemical mediators (1). Both structural and functional aspects of this adaptive immune receptor system have parallels with B cell and T cell receptors for antigen, all of which utilize ligand-induced receptor clustering as a key step in signal initiation (8,9).

Despite a wealth of information currently available about the molecular components of signaling pathways in many cell types, relatively little is known how these are spatially regulated within the cell. Multivalent protein conjugates such as 2, 4-dinitrophenyl-modified bovine serum albumin (DNP-BSA) have been useful for evaluating signal transduction in mast cells stimulated by FcεRI receptors that are sensitized with anti-DNP IgE. However, binding and crosslinking mediated by these multivalent ligands is complicated (10), and the intrinsic heterogeneity of the complexes formed do not allow studies aimed at examining spatial consequences of signaling initiated by the engaged receptors. Previous studies showed that bivalent DNP ligands with relatively short (< 5nm) flexible spacers are ineffective stimulators of mast cell degranulation, in part because of efficient formation of cyclic dimers of IgE receptor complexes (11,12). Long flexible spacers in the range of 10 nm were found to crosslink effectively the two binding sites of IgE intramolecularly and thereby to inhibit intermolecular IgE crosslinking (13). To address more directly the structural constraints in crosslinked IgE-FcεRI and resulting signaling complexes, bivalent ligands with rigid spacers were made with double-stranded DNA (dsDNA), which has a persistence length of ~50 nm (14). These ligands were found to stimulate some degranulation and also revealed a length-dependence, such that bivalent ligands with rigid spacers of 4 $-$5 nm were more effective than longer ligands of the same structure (15). However, detailed analysis of early signaling events stimulated by these variable length ligands was limited by the overall low level of responses elicited.

Because trimeric and larger crosslinking of IgE-receptors are known to cause significantly higher levels of cellular responses (16), we took advantage of branched dsDNA constructions (17,18). In particular, we synthesized and characterized a series of Y-shaped trivalent ligands with rigid dsDNA scaffolding and arms of different lengths to examine structural constraints in signaling. Like linear dsDNA, these versatile scaffolds can be stochiometrically labeled with DNP (or other groups) at the 5' end of each strand separately, and then annealed to form the branched dsDNA structure. Thus, these Y-shaped scaffolds can be made selectively mono-, di-, or tri-valent with DNP, or alternatively, fluorescent probes can be attached for imaging or for resonance energy transfer measurements of distances. We find that the trivalent Yn-DNP$_3$ ligands trigger robust signaling responses. Stimulated phosphorylation of FcεRI subunits and LAT by Lyn as well as other responses leading to degranulation are dependent on ligand length. However, another pathway leading to Ca^{2+} release from intracellular stores does not show this length dependence. Our results with these novel ligands provide a new view of spatial regulation involved in the earliest steps in FcεRI signal transduction.

RESULTS AND DISCUSSION

Construction of Y-shaped dsDNA Ligands (Yn-DNP$_3$)

To address structural constraints in receptor mediated signaling, we prepared and characterized a series of trivalent ligands of different lengths, in which dsDNA provides a rigid, Y-shaped spacer between DNP haptens conjugated at the 5'-terminus of each arm via a flexible linker (Figure 1a). DNA sequences (Supplemental Table S1) were selected for maximal hybridization stability based on previous studies (17,18). Conjugated DNP-DNA single strands were purified by HPLC (Supplemental Figure S1), and then annealed to yield trimeric molecules as confirmed by gel electrophoresis (Figure 1b). Scaffolds were also prepared with 5' ends selectively labeled with probes for fluorescence resonance energy transfer to measure the corresponding distances and to assess shape. These measurements confirmed the Y-shaped scaffolds to be rigid although moderately aplanar and asymmetric (JB Lee et al, in preparation). Dimensions and binding properties of four different trivalent DNP ligands (Yn-DNP$_3$; n= 16, 26, 36, 46 bases per single strand) are listed in Table 1. Average distances between 5' termini reflect the measured aplanarity. When bound to anti-DNP IgE, the DNP and the linker are mostly contained within the IgE binding site (19), such that the distance between two simultaneously bound IgE is determined largely by the distance between 5' ends of the dsDNA scaffold (see Figure 1c). Because of the rigid asymmetric scaffold, the distances between pairs of the three 5' ends for each Yn-DNP$_3$ vary over a limited range. Although exact distances cannot be determined, comparing responses of the four Yn-DNP$_3$ ligands of progressively longer lengths allows the question of Structural constraints in IgE-FcεRI signaling to be addressed systematically.

Binding of the Yn-DNP$_3$ ligands to anti-DNP IgE was evaluated by equilibrium titrations with FITC-modified anti-DNP IgE in solution, as well as for the same IgE bound to FcεRI on RBL mast cells. The data were fitted to a simple binding model that yields a single apparent dissociation constant K_d (19;Table 1), which serves as a measure of avidity. All four trivalent ligands bind with similar avidity to IgE in solution (Supplemental Fig S2a), yielding $K_d = 3.0-4.0$ nM (Table 1). For FITC-anti-DNP IgE bound to FcεRI on cells, significantly tighter binding (K_d ~1.5 nM) is observed that is similar for all of these ligands (Supplemental Fig S2a;Table 1). The values of K_d measured for these ligands, both on cells and in solution, are substantially smaller than for monovalent DNP-dsDNA ligands with the same scaffolding structure, K_d ~10−20 nM (15). These results indicate efficient crosslinking of anti-DNP IgE by all of the trivalent Yn-DNP$_3$, especially for IgE confined to the cell surface, where the apparent K_d is about 10-fold smaller than that observed for monovalent binding. When examined by confocal microscopy, cells sensitized with Alexa488-IgE and incubated with the Yn-DNP$_3$ showed only limited patching of labeled IgE-FcεRI complexes that was similar for the four lengths of Yn-DNP$_3$ (data not shown). We also investigated ligand-mediated internalization of FcεRI as measured with FITC-IgE that undergoes fluorescence quenching within the acidic environment of endosomes. The Yn-DNP$_3$ did not induce internalization detectably for any of these ligands, similar to previous observations with other ligands of limited valency (20).

To compare directly the extents of intermolecular crosslinking and size distributions of IgE complexes with these trivalent ligands, we employed HPLC gel permeation chromatography. Soluble IgE bound to YnDNP$_3$ elutes as a broader band at shorter retention times than unliganded IgE (Supplemental Fig S3b), indicating the existence of higher molecular weight complexes. By comparison with molecular weight markers, these appear to be chiefly trimers and tetramers of IgE bound with each of the trivalent species. These results are consistent with efficient binding of all of the Yn-DNP$_3$ ligands to anti-DNP IgE, as expected from the equilibrium binding studies, and they demonstrate that all of these ligands are effective intermolecular crosslinkers of anti-DNP IgE in solution. Figure 1c

shows a schematic of IgE-FcεRI complexes crosslinked on the cell surface by the rigid YnDNP$_3$.

Cellular degranulation stimulated by the Yn-DNP$_3$ ligands depends on spacer length

We first compared the dose dependence of the degranulation response. Fig 2a shows a single representative experiment that directly compares all four of the Yn-DNP$_3$ ligands. For the shorter ligands, Y16-DNP$_3$, Y26-DNP$_3$ and Y36-DNP$_3$, the maximal degranulation response is observed at 30nM of Yn-DNP$_3$ (90 nM DNP), and these three exhibit similar magnitudes, with an average of $20 \pm 5\%$ at this dose in multiple comparative experiments. In the same experiments, multivalent DNP-BSA stimulated an average response of 50−60% at its optimal dose of ~ 1.5 nM of BSA(~ 15 DNP per BSA molecule). For the longest trivalent ligand, Y46-DNP$_3$, degranulation is stimulated to a substantially smaller extent than for the three shorter trivalent ligands, and this is detectable only at very high doses (e.g., 300 nM Y46-DNP$_3$ in Fig 2a).

We also compared these responses in the presence of cytochalasin D, an inhibitor of actin polymerization that is known to enhance degranulation responses, particularly for small, synthetic ligands (21). Fig 2b shows a representative experiment that compares the Yn-DNP$_3$ ligands. As expected, stimulated degranulation responses are enhanced, and similar dose dependencies are observed as in the absence of cytochalasin D. For Y16-DNP$_3$, Y26-DNP$_3$ and Y36-DNP$_3$, the maximal degranulation response observed is $65 \pm 10\%$ at 30 nM Yn-DNP$_3$ for multiple independent experiments, and this is very similar to the maximal response of $70 \pm 5\%$ stimulated by multivalent DNP-BSA. All these Yn-DNP$_3$ ligands triggered reduced degranulation at the highest ligand concentrations tested, consistent with reduced crosslinking that corresponds to increased monovalent binding (22). The degranulation response to Y46-DNP$_3$ is substantially smaller than that for the other trivalent ligands at all doses tested, as is the case in the absence of cytochalasin D (Fig 2a). Because this longest trivalent ligand exhibits binding and intermolecular crosslinking of anti-DNP IgE similar to the shorter Yn-DNP$_3$, these results indicate that this ligand forms a crosslinked complex that is limited in its signaling capacity by spacer lengths exceeding 12 nm (Table 1).

Yn-DN$_3$ ligands stimulate length-dependent early tyrosine phosphorylation responses

The earliest transmembrane signaling event stimulated by ligands that effectively crosslink IgE is tyrosine phosphorylation of FcεRI by Lyn kinase. Fig 3a shows representative western blots of stimulated tyrosine phosphorylation of immunoprecipitated FcεRI β and γ subunits, carried out under conditions of maximal activation by the Yn-DNP$_3$ ligands. Fig 3b-c show quantitative analysis of western blots of these phosphorylated proteins, from several independent experiments, each normalized with respect to stimulation by the shortest ligand, Y16-DNP$_3$. Progressively smaller responses with increasing length of the trivalent ligands are observed, such that phosphorylation of each of FcεRI β and γ stimulated by the longest ligand, Y46-DNP$_3$, is five to tenfold less than that stimulated by Y16-DNP$_3$. These responses are all substantially smaller than that stimulated by 1.5 μM DNP-BSA, which is ~3-fold larger than the response to Y16-DNP$_3$ (data not shown). The time course The kinetics of receptor tyrosine phosphorylation stimulated by the Yn-DNP$_3$ was also investigated. Figure 3d compares the time courses for summarizes the results of time-based tyrosine phosphorylation of FcεRIβ and FcεRIγ , stimulated by Y16-DNP$_3$ and Y46-DNP$_3$ in the same experiment. For both ligands, maximal phosphorylation occurs within the first 2−3 minutes, and the magnitude of phosphorylation subsequently diminishes to near baseline after 10 min of stimulation. The results show that Y46-DNP$_3$ stimulates less tyrosine phosphorylation than does Y16-DNP$_3$ at every time point. Other experiments

confirmed similar length-dependent trends in stimulated tyrosine phosphorylation for varying ligand doses and stimulation times (data not shown)

These results indicate that Lyn-mediated phosphorylation of FcεRI depends on the length of the spacer between crosslinked IgE-FcεRI complexes, and this is consistent with previous evidence that transphosphorylation is key for the effectiveness of this step (4). It is known that the β subunit of FcεRI serves as a signal amplifier, and antigen-stimulated tyrosine phosphorylation overall is significantly reduced in its absence (23). Thus, FcεRI is initially phosphorylated in subunit β-ITAM motifs by non-bound Lyn in lipid rafts that are stabilized by receptor crosslinking. Then, Lyn binds via its SH2 domains to phosphorylated β, and in this position effectively facilitates amplified phosphorylation of juxtaposed FcεRI-β and -γ in the ligand-crosslinked complex. A longer enforced distance would be expected to reduce the probability of transphosphorylation of FcεRI-β and -γ, as observed for the increasing spacer lengths of Yn-DNP$_3$ (Fig 3,Table 1). Our data support a model in which constraining the crosslinked complexes to extended structures with longer spacing between IgE binding sites markedly reduces the amplification of FcεRI phosphorylation by FcεRI β that is also manifested in significantly reduced degranulation (Fig 2). Also consistent with this model are our results with P815 mast cells expressing human FcεRI α and mouse FcεRI γ$_2$ in the absence of FcεRI β (24). We find that stimulated tyrosine phosphorylation and calcium responses in these cells are independent of Yn-DNP$_3$ length and equivalent to responses stimulated by multivalent antigen (unpublished results).

Lyn bound to FcεRI also phosphorylates and thereby activates Syk after the latter kinase binds via its tandem SH2 domains to the phosphorylated ITAM motifs in FcεRI-γ (5). Fig 3a, d shows that phosphorylation of LAT also depends on the length of the spacer between crosslinked IgE-FcεRI complexes. Reduction in the phosphorylation of FcεRI-βγ likely limits the recruitment of Syk. This would in turn limit phosphorylation and activation of transmembrane adaptor protein LAT, which depends on Syk kinase (25). These propagating effects are consistent with our observations of ligand length dependence, with the longest ligand Y46-DNP$_3$ stimulating the weakest phosphorylation of LAT. Other structural constraints imposed by rigid ligand length are possible; for example, this step may also involve transphosphorylation of LAT by Syk within an FcεRI-assembled complex.

We also evaluated analogous bivalent ligands Yn-DNP$_2$ with only two of the three 5' ends conjugated to DNP. These showed only low amounts of phosphorylation and negligible degranulation activity, consistent with earlier observations that dimeric crosslinking and linear chains or cycles of IgE-FcεRI are generally ineffective for cell activation (15).

Calcium mobilization stimulated by Yn-DNP$_3$ligands varies with spacer length

The ligand length dependence of early signaling events and of degranulation predicts that Ca^{2+} mobilization, which is necessary for stimulated exocytosis, would exhibit similar differences. In fact, stimulated Ca^{2+} mobilization results from multiple processes, including IP$_3$ mediated release from intracellular (endoplasmic reticulum) stores and store-operated Ca^{2+} influx from the extracellular medium. Fig 4a compares representative time courses for Ca^{2+} mobilization stimulated by the Yn-DNP$_3$ ligands and multivalent DNP-BSA when cells are incubated in medium containing millimolar Ca^{2+}. Fig 4b quantifies these time-integrated Ca^{2+} responses stimulated by the Yn-DNP$_3$ ligands from several experiments. The response stimulated by Y16-DNP$_3$ shows a biphasic time course similar to that observed for multivalent antigen, in which rapid Ca^{2+} release from intracellular stores contributes to the initial increase in cytoplasmic Ca^{2+}, followed by a slow decline in the sustained phase that is due to the store-operated Ca^{2+} influx from the external medium (Fig 4a; ref 26). The Y26-DNP$_3$ and Y36-DNP$_3$ ligands exhibit more slowly developing Ca^{2+} responses that eventually exceed the magnitude of the sustained influx phase stimulated by

Y16-DNP$_3$. These three shorter Yn-DNP$_3$ ligands stimulate similar net Ca^{2+} mobilization as integrated over 600 sec after the stimulus (Fig 4b). In contrast to these substantial Ca^{2+} responses, the longest ligand, Y46-DNP$_3$, stimulates only a very small and slowly developing response (Fig 4 a, b), consistent with its inefficient stimulation of early phosphorylation events (Fig 3) and degranulation (Fig 2).

We also compared the calcium responses to Yn-DNP$_3$ ligands in presence of cytochalasin D and our results indicate that the magnitude of the time-integrated responses ligand mediated calcium response increases by about 20 % compared to those in the absence of cytochalasin D (data not shown). Consistent with our degranulation results, the longest ligand Y46-DNP$_3$ stimulates only a very small calcium response compared to the other Yn-DNP$_3$ under these conditions (data not shown).

To investigate the basis for these differences in overall Ca^{2+} mobilization, we evaluated the ligand-stimulated release of Ca^{2+} from intracellular stores that can be observed in the absence of extracellular Ca^{2+} (27). As seen in Fig 5a, the shortest ligand, Y16-DNP$_3$, stimulates a large, rapid release of Ca^{2+} from stores similar to that evoked by a multivalent antigen (Fig 4a, top left panel). All of the longer ligands, Y26-DNP$_3$, Y36-DNP$_3$, and Y46-DNP$_3$ exhibit responses similar to each other. These are all slower than that for Y16-DNP$_3$, but the net stimulated release from stores is similar for all the Yn-DNP$_3$ when integrated over 300 sec after addition of stimulus (Fig 5b). This trend is not altered when release from stores in integrated over longer times (data not shown). Thus, stimulated Ca^{2+} release from stores does not exhibit the same ligand length dependence observed for the other responses evaluated (Figs 2, 3), including Ca^{2+} mobilization in the presence of extracellular Ca^{2+} that is largely a manifestation of Ca^{2+} influx (Fig 4).

Previous studies showed that antigen-stimulated production of IP$_3$ by activated PLCγ is the principal mechanism by which store-operated Ca^{+2} influx is initiated in these cells (28,29) activation of PLCγ1 and PLCγ2 by crosslinked FcεRI depends on stimulated tyrosine phosphorylation of these enzymes (7), so we compared the Yn-DNP$_3$ to evaluate the ligand length dependence. Fig 5c shows a representative western blot of ligand-stimulated tyrosine phosphorylation of PLCγ1 under optimal conditions, with anti-PLCγ1 reprobe to confirm similar loading for all samples (Fig 5d). Fig 5e quantifies this blot together with those from several other experiments of similar design and shows that PLCγ1 phosphorylation is not significantly different for Yn-DNP$_3$ of different lengths. Similar results were obtained for PLCγ2 (data not shown). These results are consistent with the ligand length independence of Ca^{2+} release from stores (Fig 5b). Overall, these results reveal that PLCγdependent, IP$_3$-mediated Ca^{2+} release from intracellular stores, stimulated by Yn-DNP$_3$ ligands, utilizes a pathway that is distinguishable from ligand length-dependent Syk kinase phosphorylation of LAT.

It is interesting that while both LAT and PLCγ1 can be phosphorylated by Syk kinase (25), Yn-DNP$_3$ stimulation of LAT phosphorylation depends on ligand length (Fig 3) whereas PLCγ1 phosphorylation does not (Fig 5). A possible explanation is that PLCγ1 phosphorylation stimulated by Yn-DNP$_3$ is mediated by Bruton's Tyrosine Kinase (Btk), a member of the Tek kinase family that has also been shown to phosphorylate PLCγ in response to FcεRI signaling (30). Btk can be activated by Lyn-mediated phosphorylation, but this may not involve transphosphorylation with strict structural constraints in an assembled FcεRI complex. In bone marrow-derived mouse mast cells, an alternative Fyn kinase-dependent pathway for Btk activation involving PI3 kinase and Btk (but not Syk or LAT) has been described (1), and this may be responsible for PLCγ activation by Yn-DNP$_3$.

To evaluate the role of PI3 kinase in PLCγ activation by the Yn-DNP$_3$ ligands, we examined the effect of 200 nM wortmannin on the release of Ca^{2+} from intracellular stores. At this concentration, wortmannin selectively and irreversibly inhibits all PI3 kinase isoforms (31). As shown in Figure 6a and b, wortmannin almost completely inhibits Ca^{2+} release from stores that is stimulated by both Y16-DNP$_3$ and Y46-DNP$_3$, whereas it only slightly inhibits this response stimulated by multivalent antigen (Fig 6c). In contrast, 1 μM U73122, which is highly specific for PLCγ, completely inhibits Ca^{2+} release from stores that is stimulated by all three ligands (Figure 6), indicating the dependence of this process on IP$_3$ production for all three. These results indicate a substantial difference in the mechanism of PLCγ activation leading to IP$_3$ production for the Yn-DNP$_3$ ligands compared with that for multivalent DNP-BSA. Tyrosine phosphorylation, including that of LAT, stimulated by any of the Yn-DNP$_3$ ligands is substantially smaller than is stimulated by DNP-BSA, and the lower level of LAT phosphorylation may be insufficient to cause significant PLCγ activation. Thus, for these trivalent ligands, PI3 kinase-dependent activation of PLCγ is apparently dominant, and does not utilize the Lyn/Syk/LAT axis. These results provide additional evidence that this axis of signaling is selectively affected by restricted spacing between the crosslinked IgE-FcεRI.

Together, Figs 4 and 6 indicate that the ligand length dependence of Ca^{2+} mobilization is due to differences in the activation of Ca^{2+} influx. Recent studies demonstrated that the Ca^{2+} sensor protein STIM1 redistributes within the endoplasmic reticulum to contact the plasma membrane, where it engages to activate the store-operated Ca^{2+} influx channel, CRACM1 (32,33). This process depends on the emptying of intracellular Ca^{2+} stores by IP$_3$, and other processes such as vesicle trafficking to the plasma membrane may occur. Our results show that Yn-DNP$_3$-stimulated Ca^{2+} influx requires signaling events in addition to IP$_3$ production that are sensitive to spacing between the ligand-clustered IgE-FcεRI.

Summary and Conclusions

The Yn-DNP$_3$ ligands with rigid spacers developed for this study reveal structural constraints within the receptor-protein assemblies that transduce signaling across the cellular membrane due to crosslinking of IgE-FcεRI. Phosphorylation of FcεRI and subunits by Lyn progressively decreases as the spacer length increases from about 5 nm (Y16-DNP$_3$) to more than 12 nm (Y46- DNP$_3$) providing direct evidence for an amplifying transphosphorylation step in the mechanism. These spacer lengths range from a little more than one to three immunoglobulin domain lengths (Fig 1c), and the longest ligand is likely to prevent direct contact between crosslinked IgE receptor complexes. Syk kinase dependent phosphorylation of LAT shows a similar length dependence that could include contributions from Lyn-Syk transphosphorylation or Syk-LAT transphosphorylation in the crosslinked receptor complex that assembles. The Ca^{2+} mobilization and cellular degranulation that result from the early phosphorylation events also show ligand length dependence with the difference that the ligand with the longest spacing, Y46-DNP$_3$ (average 13 nm), stimulates substantially less activity than the shorter three Yn-DNP$_3$, (averages $5 - 10$ nm) suggesting a threshold in the level of transphosphorylation necessary for downstream signaling and/or additional structural constraints in this pathway. Our results with the Yn-DNP$_3$ ligands also reveal that Syk kinase-dependent phosphorylation of LAT leading to Ca^{2+} mobilization and cellular degranulation can be distinguished from PLCγ-dependent, IP$_3$-mediated Ca^{2+} release from intracellular stores, based on their differential dependence on the spacing between the crosslinked IgE-FcεRI.

These ligands that are based on rigid, Y-shaped dsDNA scaffolds have proven their value in the model IgE-FcεRI system we have examined: they are defined ligands that stimulate strong cellular responses, and they enable structural constraints and structurally distinguishable signaling pathways to be revealed. With other selected groups conjugated to

their 5' ends, we expect these scaffolds will provide a useful and versatile approach for examining a broad range of receptor-mediated signaling systems.

MATERIALS AND METHODS

Synthesis and characterization of Yn-DNP$_3$

Oligonucleuotide sequences were selected for the Y-shaped DNA scaffolding as described by Luo *et.al* (18). The sequences used for n=16, 26, 36, and 46 are listed in Supplemental Table S1. They were commercially synthesized (Integrated DNA Technology), with a six carbon amine-modified 5' linker. Single strand oligonucleotides were coupled with a DNP-succinimidyl ester, DNP-X (Invitrogen/Molecular Probes) at the amine modified 5' end using the manufacturer supplied protocol with minor modifications. Briefly, ethanol precipitation of oligonucleotide was omitted, and the reactants were subjected to Microcon filtration (Millipore) to remove the unreacted DNP substrates. The DNP-labeled DNA and unlabeled DNA recovered from filtration were loaded onto a reverse phase C_{18} HPLC column (Waters Corp.) for purification using a linear gradient of aqueous 200 mM triethlyammonium acetate (pH 6.5) and 60:40 acetonitride/dH$_2$O. DNP-labeled DNA was detected as a well-resolved peak with absorbance at both 260nm and 360nm (13). Purified, DNP-labeled single strand DNA was spin-vacuum dried, dissolved in dH$_2$O, re-evaporated, and dissolved in 10 mM Tris-HCl, 1 mM EDTA, 135 mM NaCl, pH 8.5. Hybridization and annealing of three single strand oligonucleotides into the dsDNA, Y-shaped structures (Yn-DNP$_3$) was carried out as described previously (18). DNP: DNA ratios of Yn-DNP$_3$ ligands were found to be in the range of $2.5-2.7$, as determined by UV absorption spectroscopy using standard extinction coefficient values of dsDNA and DNP (15).

Equilibrium binding measurements

Equilibrium binding of the Yn-DNP$_3$ ligands to FITC-labeled IgE was measured using the fluorescence quenching method as previously described (19). In brief, fluorescence was monitored with a SLM 8100 fluorimeter in a time-based acquisition mode using fluorescein excitation and emission wavelengths of 490 nm and 520 nm, respectively. Equilibrium titrations in solution and with cell-bound FITC-IgE were conducted at room temperature with continuous stirring in a buffered salt solution (BSS: 20 mM HEPES, 135 mM NaCl, 1.8 mM CaCl$_2$, 1 mM MgCl$_2$, 5.6 mM glucose, pH 7.4) containing 1mg ml^{-1} of gelatin.

Size Exclusion Chromatography

To assess the crosslinking of anti-DNP IgE by the Yn-DNP$_3$ ligands, sizes and distributions of complexes formed in solution were analyzed with gel permeation chromatography. A 2-fold molar excess of Yn-DNP$_3$ was incubated with 1 μM anti-DNP IgE for 45 min at room temperature, then 100 μL was chromatographed on a 10mm × 300 mm column of Superose 6 (GE Healthcare) equilibrated in borate buffered saline (pH 8.2) at a rate of 0.4 mL min^{-1}. Protein absorbance was monitored at 280 nm. Gel filtration molecular weight standards (Biorad)

Cell culture and degranulation measurements

RBL-2H3 cells were maintained and passaged as previously described (34). Cells were sensitized with anti-DNP IgE at a final concentration of 1μg ml^{-1} and plated at a density of 2.5×10^5 cells well^{-1} in a 96-well plate overnight at 37°C. Adherent cells were washed in BSS containing 1mg/ml of BSA, and Yn-DNP$_3$ ligands or multivalent DNP-BSA (10) were added to the cells at indicated doses in presence and absence of 2 μM cytochalasin D. After 1 hr at 37°C, aliquots of supernatants was taken from each well to assay the extent of β-hexosaminidase release from the cells as previously described (34). Stimulated

degranulation is expressed as a percentage of the total cellular β-hexosaminidase activity present in cell lysates after solubilization in 1% Triton X-100.

Immunoprecipitation and western blotting

Immunoprecipitations were carried out as previously described (35). In brief, RBL-2H3 cells were sensitized with excess anti-DNP IgE (1 μg ml^{-1}) overnight, then cells were harvested with trypsin-EDTA, washed with BSS containing 1μg ml^{-1} BSA, and resuspended at 6.2 × 10^6 cells ml^{-1}. Cells were stimulated with Yn-DNP$_3$ ligands (or not), then aliquots of the cell suspensions were added to ice-cold 3X solubilizing buffer in a 2:1 ratio (final concentration: 0.5% Triton-X100, 50 mM Tris, 50 mM NaCl, 5 mM EDTA, 1mM Na$_3$VO$_4$, 5mM Na$_4$P$_2$O$_7$, 50mM NaF, 2 mM iodoacetate, 1 mM PMSF along with 10 μg ml^{-1} of leupeptin, aprotinin and pepstatin A (pH 7.6) or a protease inhibitor cocktail (Sigma). After incubation for 15 min at 4°C and centrifugation (11500g, 7min, 4°C), IgE-FcεRI, LAT or PLCγ was immunoprecipitated from supernatant cell lysates with the relevant purified antibody and protein A Sepharose beads (GE Healthcare). For IgE-FcεRI, rabbit anti-IgE (2 μg/ml, a gift of Dr. C. Torigoe) was used; for LAT, rabbit anti-LAT (a gift of Dr. L. Samelson, NIH) was used at 25 μg ml^{-1}, and for PLCγ1, rabbit anti-PLCγ1(#1249; Santa Cruz Biotech.) was used. Immunoprecipitated proteins were then extracted with 2X hot SDS sample buffer (Invitrogen Inc.) under reducing condition for PLCγ1 and loaded on 12% polyacrlamide gels (Invitrogen Inc.).

For anti-phosphotyrosine western blotting, electrophoresed proteins were electotransferred onto nitrocellulose membranes (Fisher, CA) and detected with 1 μg ml^{-1} of biotinylated anti-phosphotyrosine mAb 4G10 (Upstate Biotechnology) followed by horseradish peroxidaseconjugated avidin (Pierce Biotech) and enhanced chemiluminescence reagents (Pierce Biotech). Membranes containing PLCγ1 were stripped with 0.2M NaOH and further reprobed with anti-PLCγ1 antibody to measure the amount of loaded protein. Quantitative analysis of blots was carried out on non-saturated film using UN-SCAN-IT software (Silk Scientific) in a linear optical range. Relative intensities of bands were averaged for multiple experiments and expressed as normalized intensities±standard errors. The uncertainty in the band selected for normalization is similar to the standard errors for the other bands.

Measurement of intracellular Ca^{+2} mobilization

RBL-2H3 cells were loaded with indo-1 AM (Invitrogen/Molecular Probes) and sensitized with anti-DNP IgE (1 μg ml^{-1}) as previously described (36). Washed cells were resuspended in BSS with BSA and 0.25 mM sulfinpyrazone (Sigma) at a final concentration of 2 × 10^6 cells ml^{-1}. Indo-1 fluorescence was measured on an SLM 8100S fluorimeter in time-based acquisition mode as previously described (30). Cells were continuously stirred at 37°C in presence or absence of 2 μM cytochalasin D, and Yn-DNP$_3$ ligands or multivalent DNP-BSA was added as indicated. Time courses of indo-1 fluorescence were normalized to total signal in 0.1 % Triton X-100 minus background in the presence of excess EDTA.

Acknowledgments

REFERENCES

1. Rivera J, Gilfillan AM. Molecular regulation of mast cells activation. J. Allergy Clin. Immunol 2006;117(6):1214–1225. [PubMed: 16750977]
2. Kinet JP. The high affinity IgE receptor (FcεRI): From Physiology to pathology. Annu. Rev. Immunol 1999;17:931–972. [PubMed: 10358778]

3. Holowka D, Gosse JA, Hammond AT, Han X, Sengupta P, Smith NL, Wagenknecht-Wiesner A, Wu M, Young RM, Baird B. Lipid segregation and IgE receptor signaling: a decade of progress. Biochim. Biophys. Acta 2005;1746(3):252–259. [PubMed: 16054713]

4. Pribluda VS, Pribluda C, Metzger H. Transphosphorylation as the mechanism by which the high-affinity receptor for IgE is phosphorylated upon aggregation. PNAS 1994;91(23):11246–11250. [PubMed: 7526393]

5. El-Hillal O, Kurosaki T, Yamamura H, Kinet JP, Scharenberg AM. Syk kinase activation by a src kinase-initiated activation loop phosphorylation chain reaction. PNAS 1997;94(5):1919–1924. [PubMed: 9050880]

6. Samelson LE. Signal transduction mediated by T cell antigen receptor: The role of adapter proteins. Annu. Rev. Immunol 2002;20:371–394. [PubMed: 11861607]

7. Rhee SG. Regulation of phosphoinositide-specific phospholipase C. Annu. Rev. Biochem 2001;70:281–312. [PubMed: 11395409]

8. Metzger H. Transmembrane signaling: the joy of aggregation. J. Immunol 1992;149:14777–14787.

9. Kiessling LL, Gestwicki JE, Strong LE. Synthetic multivalent ligands as probes of signal transduction. Angew. Chem., Int. Ed 2000;45:2348–2368.

10. Xu K, Goldstein B, Holowka D, Baird B. Kinetics of multivalent antigen DNP-BSA binding to IgE-Fc epsilon RI in relationship to the stimulated tyrosine phosphorylation of Fc epsilon RI. J. Immunol 1998;160(7):3225–3235. [PubMed: 9531278]

11. Posner RG, Subramanian K, Goldstein B, Thomas J, Feder T, Holowka D, Baird B. Simultaneous cross-linking by two nontriggering bivalent ligands causes synergistic signaling of IgE Fc epsilon RI complexes. J Immunol 1995;155(7):3601–3609. [PubMed: 7561059]

12. Holowka D, Sil D, Torigoe C, Baird B. Insights into immunoglobulin E receptor signaling from structurally defined ligands. Immunol. Review 2007;217:269–279.

13. Baird EJ, Holowka D, Coates GW, Baird B. Highly effective poly(ethylene glycol) architectures for specific inhibition of immune receptor activation. Biochemistry 2003;42(44):12739–12748. [PubMed: 14596588]

14. Toth K, Sauermann V, Langowski J. DNA curvature in solution measured by fluorescence resonance energy transfer. Biochemsitry 1998;37:8173–8179.

15. Paar JM, Harris NT, Holowka D, Baird B. Bivalent ligands with rigid double-stranded DNA spacers reveal structural constraints on signaling by Fc epsilon RI. J. Immunol 2002;169(2):856–864. [PubMed: 12097389]

16. Fewtrell C, Metzger H. Larger oligomers of IgE are more effective than dimers in stimulating rat basophilic leukemia cells. J Immunol 1980;125(2):701–710. [PubMed: 7391576]

17. Seeman NC. Denovo design of sequences of nuclei acid structural engineering. J. Biomol. Struct. Dyn 1990;8:573–581. [PubMed: 2100519]

18. Li Y, Tseng YD, Kyon SY, D'Espaux L, Bunch JS, McEuen PL, Luo D. Controlled assembly of dendrimer-like DNA. Nature Materials 2004;3(1):38–42.

19. Erickson J, Kane P, Goldstein B, Holowka D, Baird B. Cross-linking of IgE receptor complexes at the surface: a fluorescence method for studying the binding of monovalent and bivalent haptens. Molecular Immunology 1986;23(7):769–781. [PubMed: 2948110]

20. Menon AK, Holowka D, Webb WW, Baird B. Cross-linking of receptor-bound IgE to aggregates larger than dimers leads to rapid immobilization. J. Cell Biol 1986;102(2):541–550. [PubMed: 2935543]

21. Harris N, Goldstein B, Holowka D, Baird B. Altered patterns of tyrosine phosphorylation and Syk activation for sterically restricted cyclic dimers of IgE-Fc RI. Biochemistry 1997;36:2237–2242. [PubMed: 9047325]

22. Puffer EB, Pontrello JK, Hollenbeck JJ, Kink JA, Kiessling LL. Activating B cell signaling with defined multivalent ligands. ACS Chem. Biol 2007;2(4):252–262. 24. [PubMed: 17432821]

23. Dombrowicz D, Lin S, Flamand V, Brini AT, Koller BH, Kinet JP. Allergyassociated FcRbeta is a molecular amplifier of IgE- and IgG-mediated in vivo responses. Immunity 1998;8(4):517–529. [PubMed: 9586641]

24. Miller L, Alber G, Varin-Blank N, Ludowyke R, Metzger H. Transmembrane signaling in P815 mastocytoma cells by transfected IgE receptors. J. Biol. Chem 1990;265(21):12444–12453. [PubMed: 2165065]

25. Zhang J, Berenstein EH, Evans RL, Siraganian RP. Transfection of Syk protein tyrosine kinase reconstitutes high affinity IgE receptor-mediated degranulation in a Syk-negative variant of rat basophilic leukemia RBL-2H3 cells. J. Exp. Med 1996;184(1):71–79. [PubMed: 8691151]

26. Beaven MA, Rogers J, Moore JP, Hesketh TR, Smith GA, Metcalfe JC. The mechanism of the calcium signal and correlation with histamine release in 2H3 cells. J. Biol. Chem 1984;259(11): 7129–7136. [PubMed: 6202691]

27. Beaven MA, Moore JP, Smith GA, Hesketh TR, Metcalfe JC. The calcium signal and phosphatidylinositol breakdown in 2H3 cells. J. Biol. Chem 1984;259(11):7137–7142. [PubMed: 6202692]

28. Meyer T, Holowka D, Stryer L. Highly cooperative opening of calcium channels by inositol 1, 4, 5-trisphosphate. Science 1988;240(4852):653–666. [PubMed: 2452482]

29. Lee HS, Park CS, Lee YM, Suk HY, Clemons TC, Choi OH. Antigen-induced Ca^{+2} mobilization in RBL-2H3 cells: role of $I(1,4,5)P_3$ and S1P and necessity of $I(1,4,5)P_3$ production. Cell Calcium 2005;38:581–592. [PubMed: 16219349]

30. Iwaki S, Tkaczyk C, Satterthwaite AB, Halcomb K, Beaven MA, Metcalfe DD, Gilfillan AM. Btk Plays a Crucial Role in the Amplification of Fc RI-mediated Mast Cell Activation by Kit. J. Biol. Chem 2005;280:40261–40270. [PubMed: 16176929]

31. Thelen M, Wymann MP, Langen H. Wortmannin binds specifically to 1-phosphatidylinositol 3-kinase while inhibiting guraranine nucleotide-binding protein-coupled receptor signaling in neutrophil leukocytes. Proc. Natl. Acad. Sci. USA 1994;91:4960–4964. [PubMed: 8197165]

32. Liou J, Kim ML, Heo WD, Jones JT, Myers JW, Ferrell JE Jr. Meyer T. STIM is a Ca2+ sensor essential for Ca2+-store-depletion-triggered Ca^{+2} influx. Current Biol 2005;15(13):1235–1241.

33. Peinelt C, Vig M, Koomoa DL, Beck A, Nadler MJ, Koblan-Huberson M, Lis A, Fleig A, Penner R, Kinet JP. Amplification of CRAC current by STIM1 and CRACM1 (Orai 1). Nat. Cell Biol 2006;8:771–773. [PubMed: 16733527]

34. Naal RM, Tabb J, Holowka D, Baird B. In situ measurement of degranulation as a biosensor based on RBL-2H3 mast cells. Biosens. Bioelectron 2004;20(4):791–796. [PubMed: 15522594]

35. Torigoe C, Metzger H. Spontaneous phosphorylation of the receptor with high affinity for IgE in transfected fibroblast. Biochemistry 2001;40:4016–4025. [PubMed: 11300782]

36. Pierini L, Harris NT, Holowka D, Baird B. Evidence Supporting a role for microfilaments in regulating the coupling between poorly dissociable IgE-FcεRI aggregates and downstream signaling pathways. Biochemistry 1997;36:7447–7456. [PubMed: 9200693]

Supplementary Material

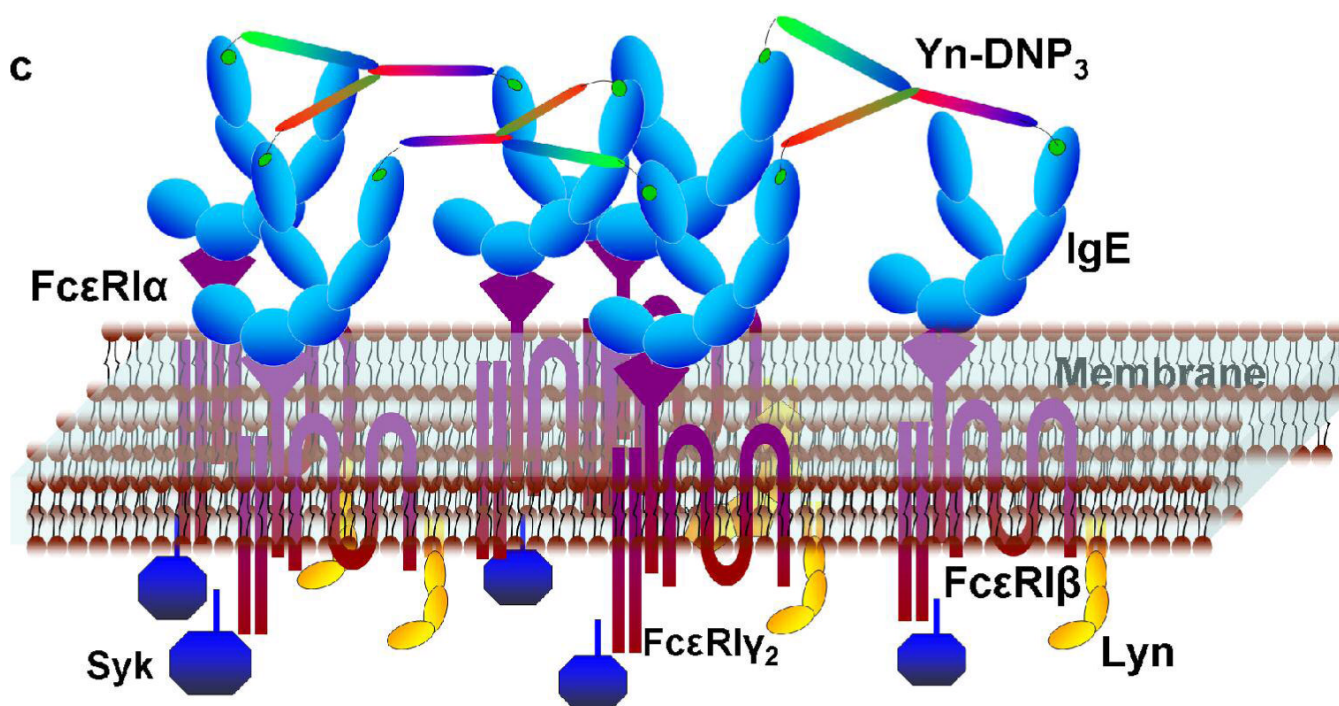Refer to Web version on PubMed Central for supplementary material.
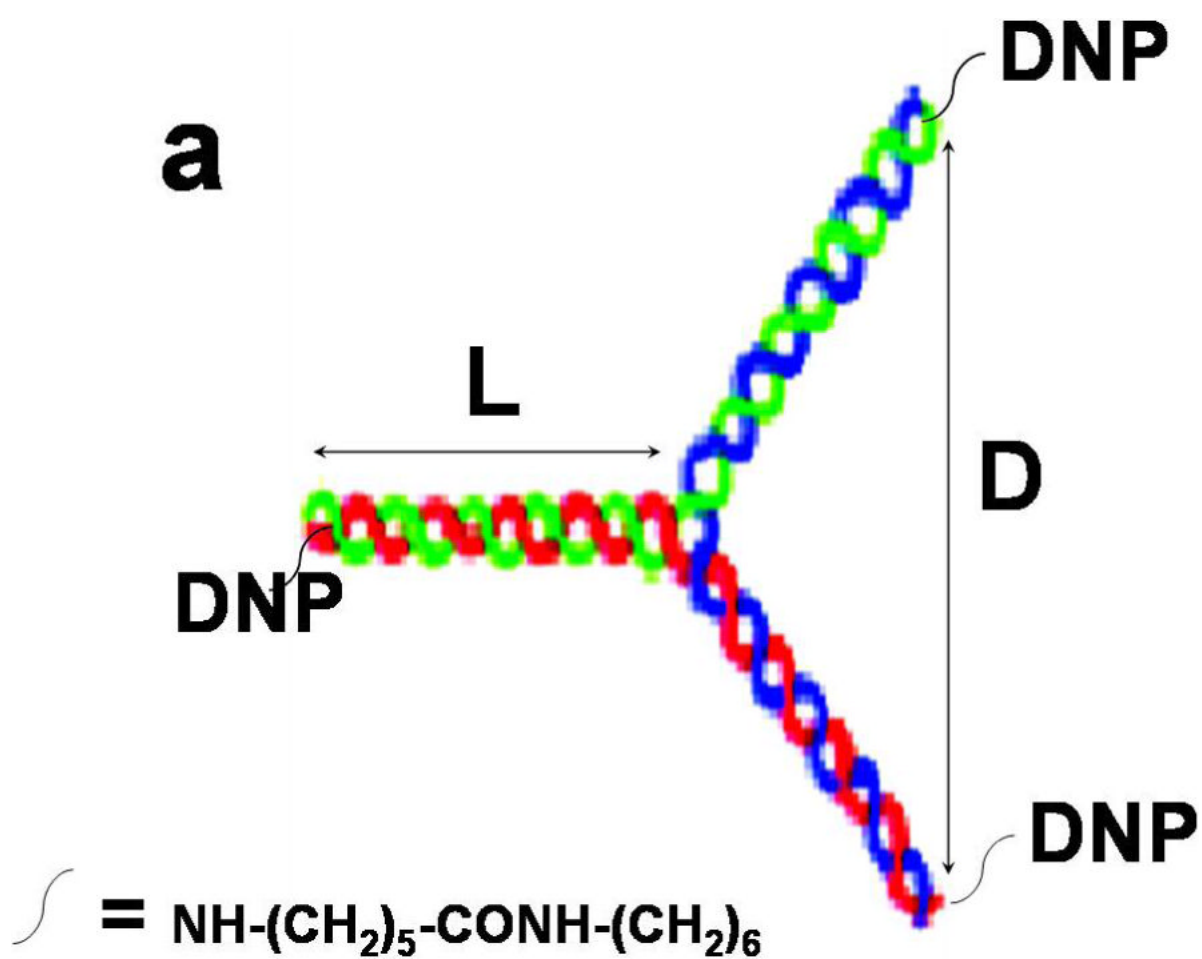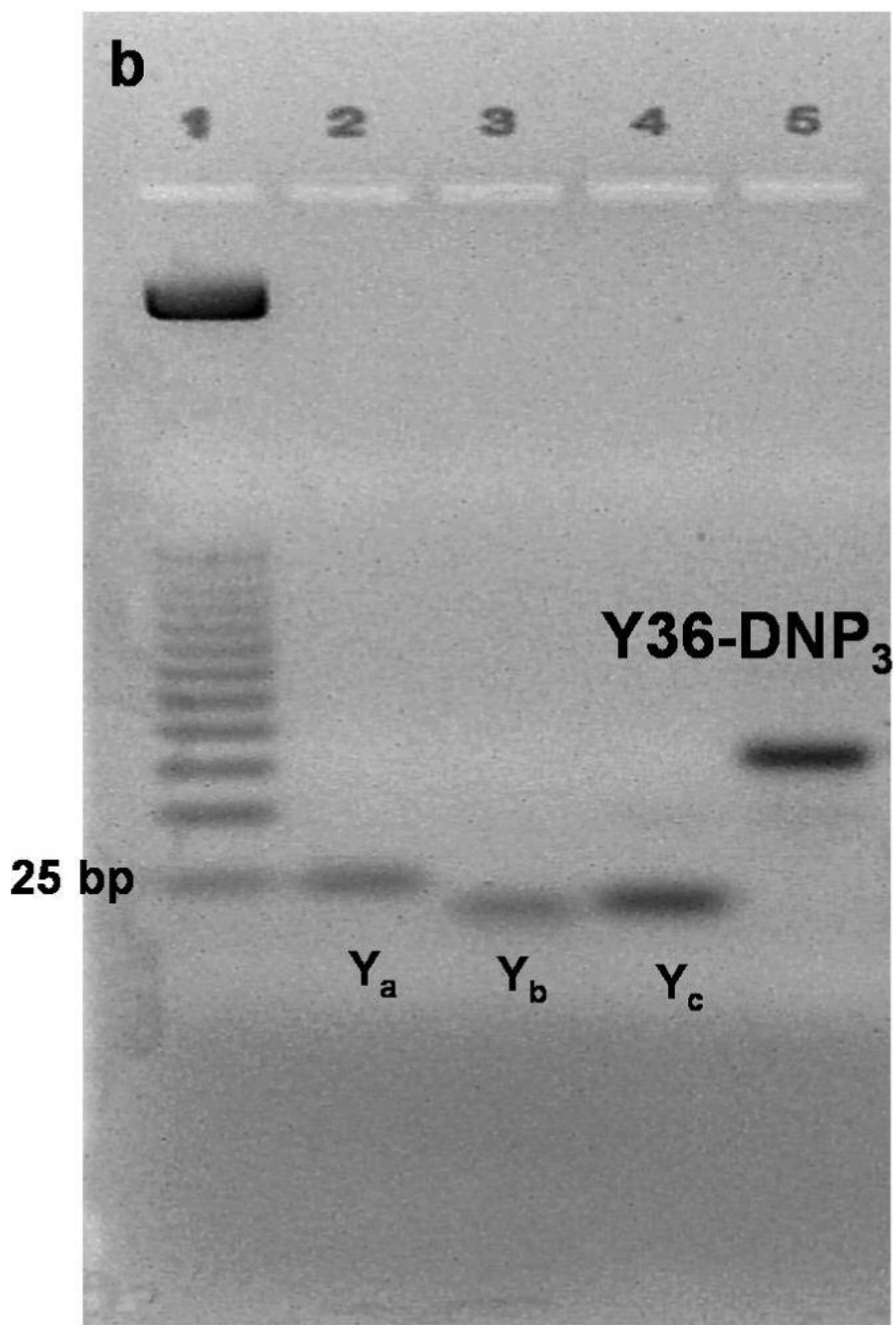
Figure 1. Schematic Structure and assembly of Yn-DNP$_3$ and cross linked IgE-FcεRI
a) The Yn-DNP$_3$ complex comprises three single nucleotide strands (blue, red, green) of selected length and sequence (Supplemental Table S1) that are first conjugated with a DNP group at the 5' end, then purified and annealed (15). Dimension *L* refers to the length of each arm, and dimension *D* refers to the distance between a pair of 5' ends. Values for each of the four Yn-DNP$_3$ ligands (n= 16, 26, 36, 46) are included in Table 1. b) Agarose gel stained with EtBr after electrophoresis of representative Y36-DNP$_3$ construct: single strands, each containing 36 nucleotides (Y$_a$, Y$_b$ and Y$_c$), and annealed, trivalent Y36-DNP$_3$. c) Schematic of IgE-FcεRI crosslinked by the rigid Yn-DNP$_3$ on the surface of RBL mast cells that leads to transmembrane coupling with signaling kinases Lyn and Syk.
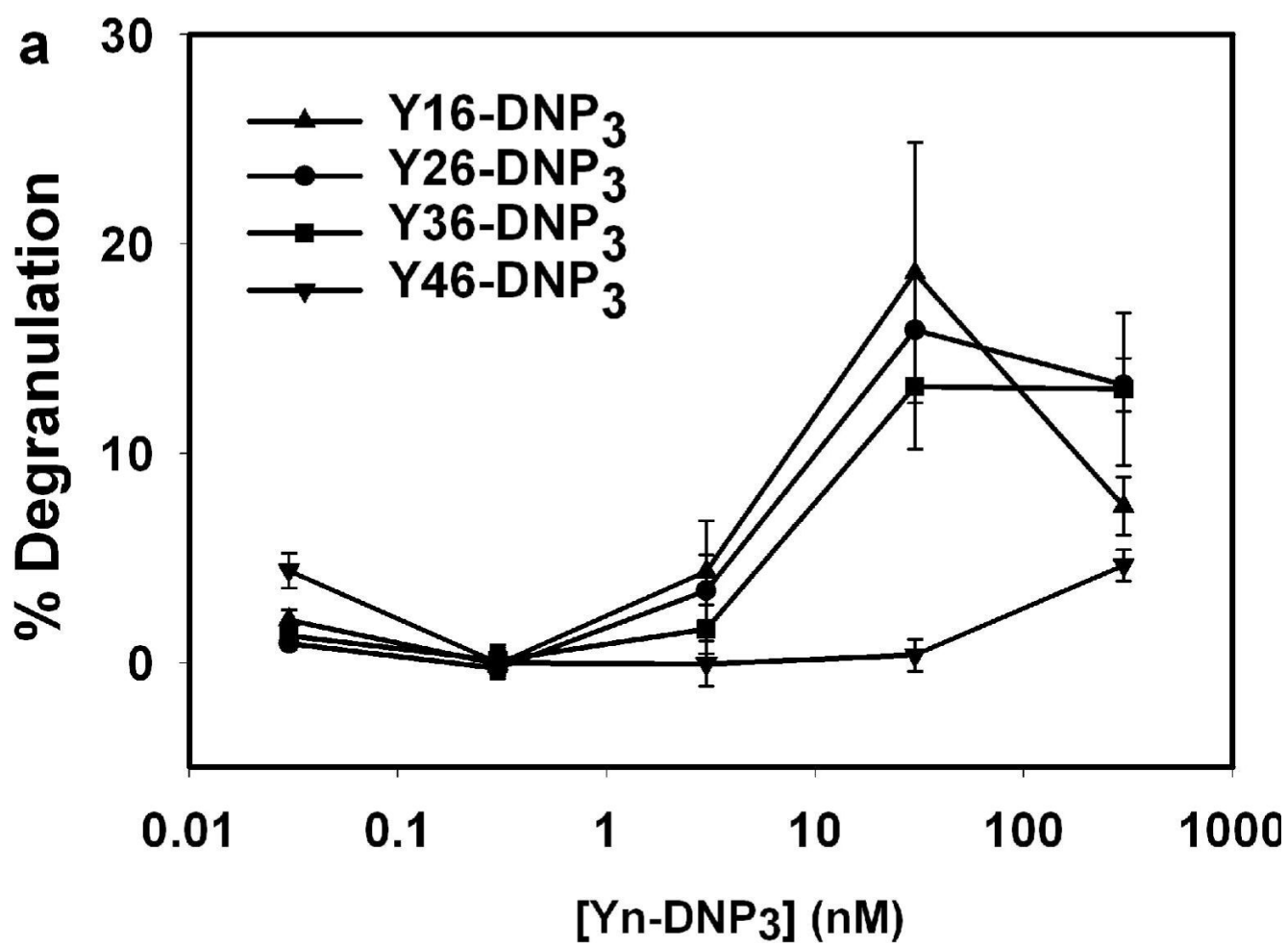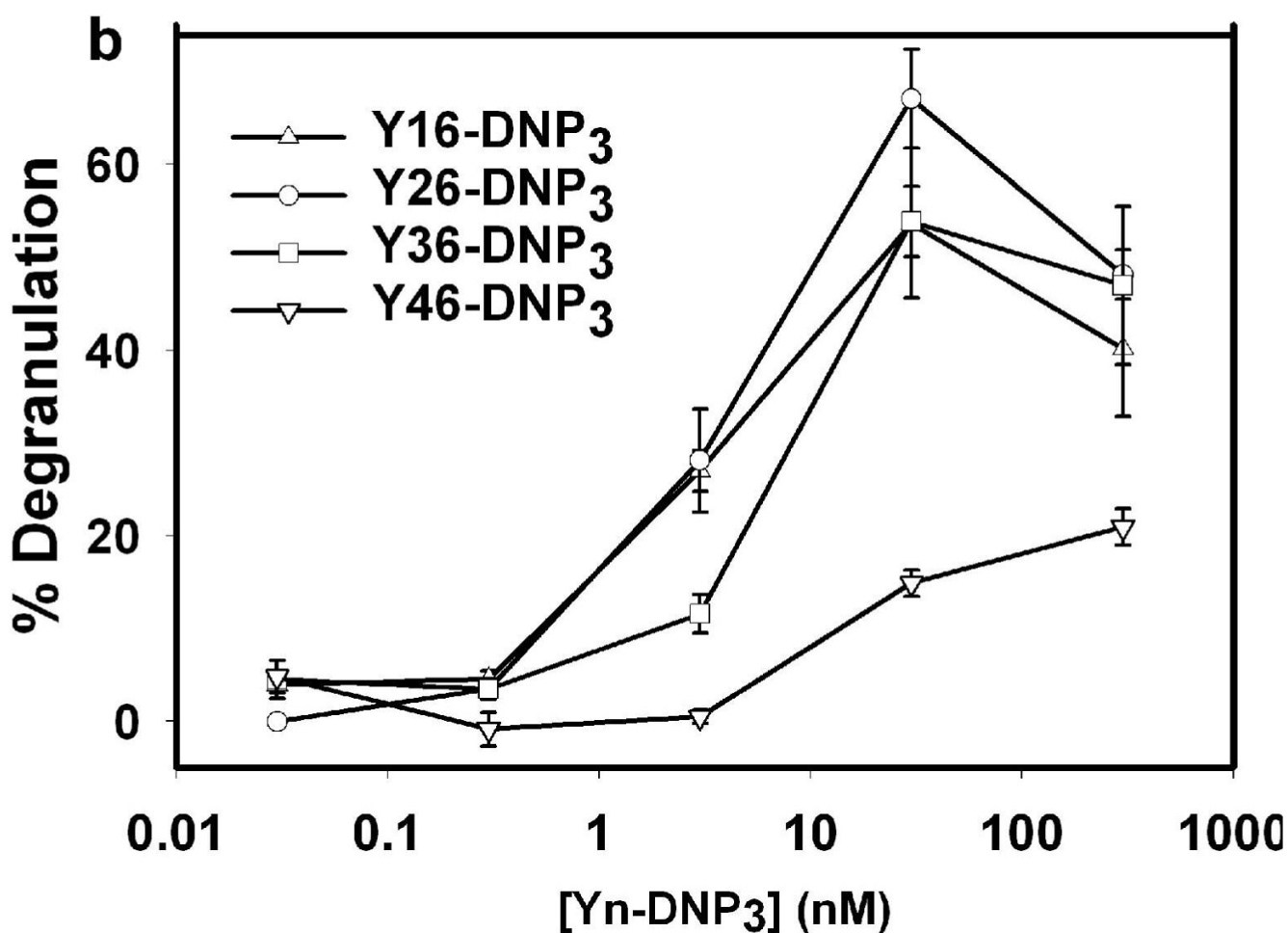
Figure 2. Degranulation of RBL-2H3 mast cells stimulated by Yn-DNP$_3$ ligands
β-Hexosaminidase release from cells after stimulation with varying doses of specified Yn-DNP$_3$ ligand in the (a) absence and (b) presence of 2 μM cytochalasin D. Data shown are from a single, comparative experiment that is representative of 5−10 different experiments with each ligand. Error bars represent range of triplicate samples. Degranulation is quantified as the percentage of total β-hexosaminidase released in TX-100 cell lysates.
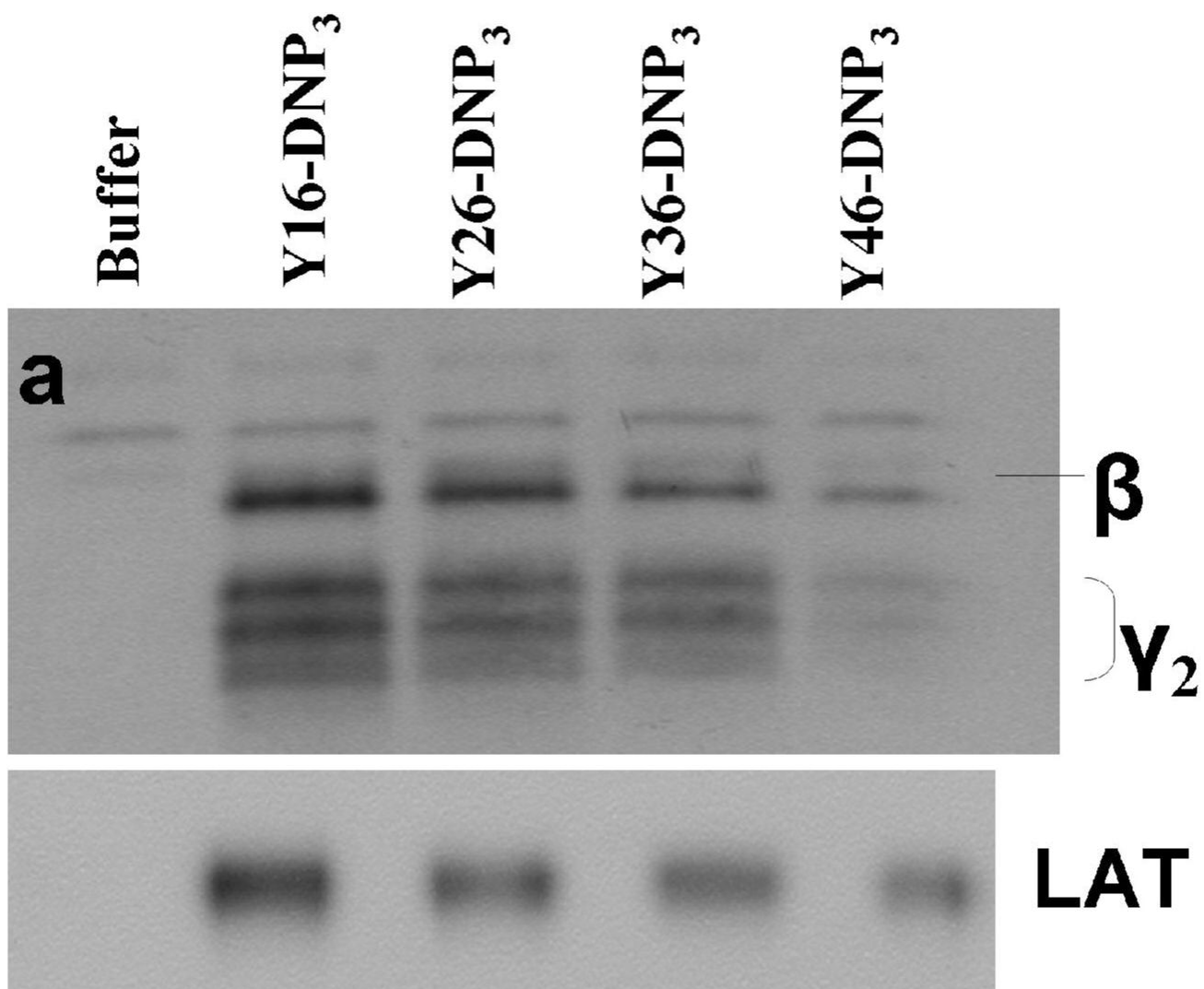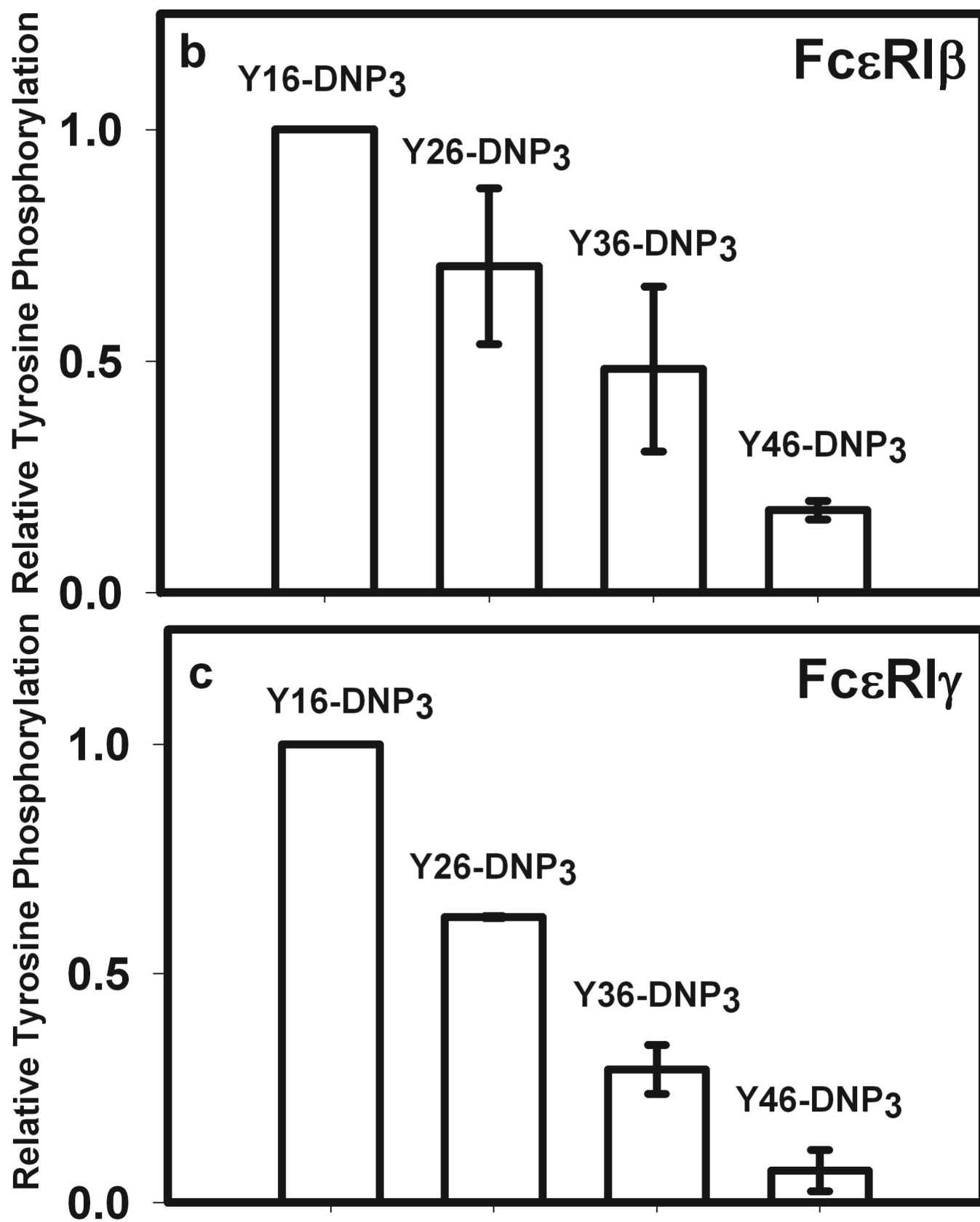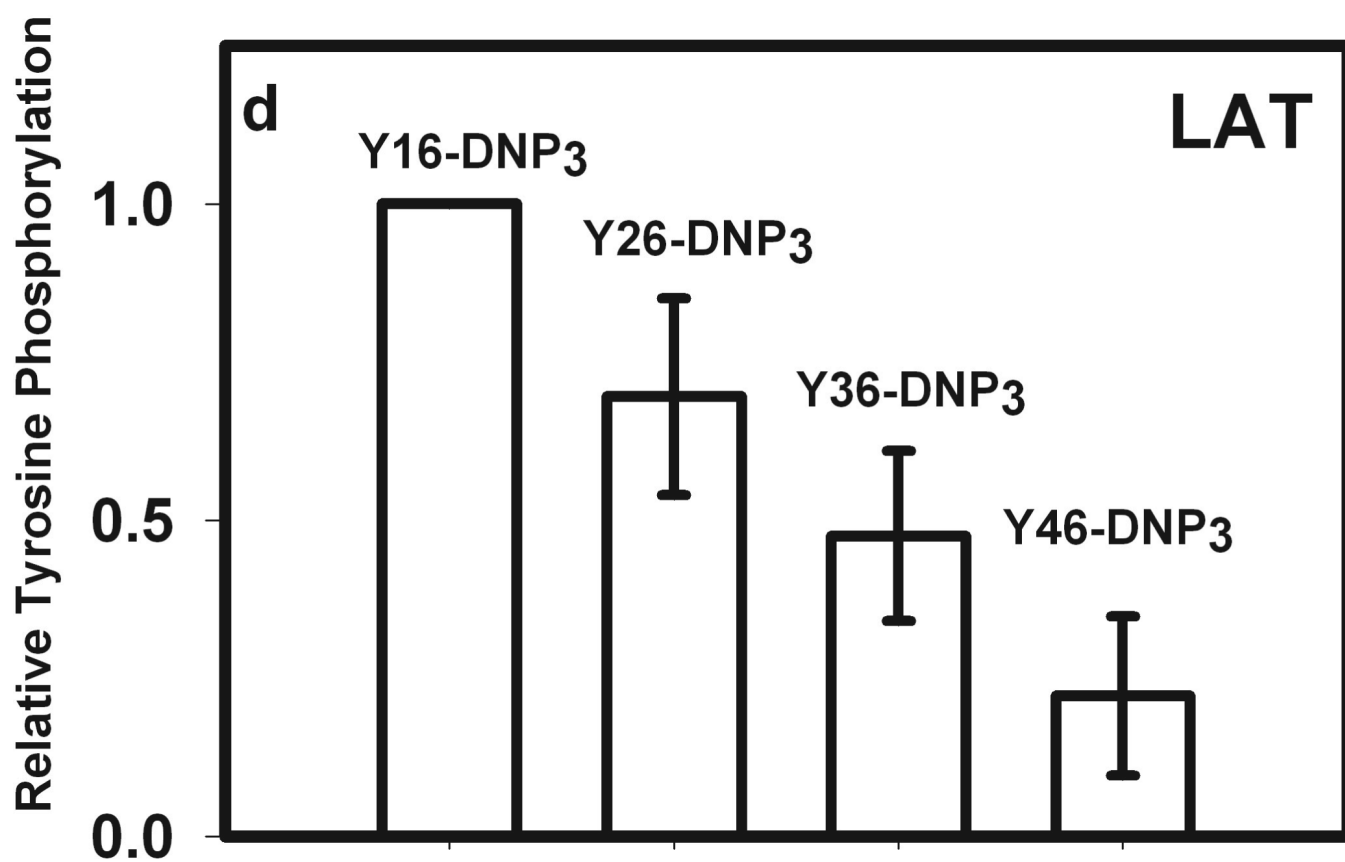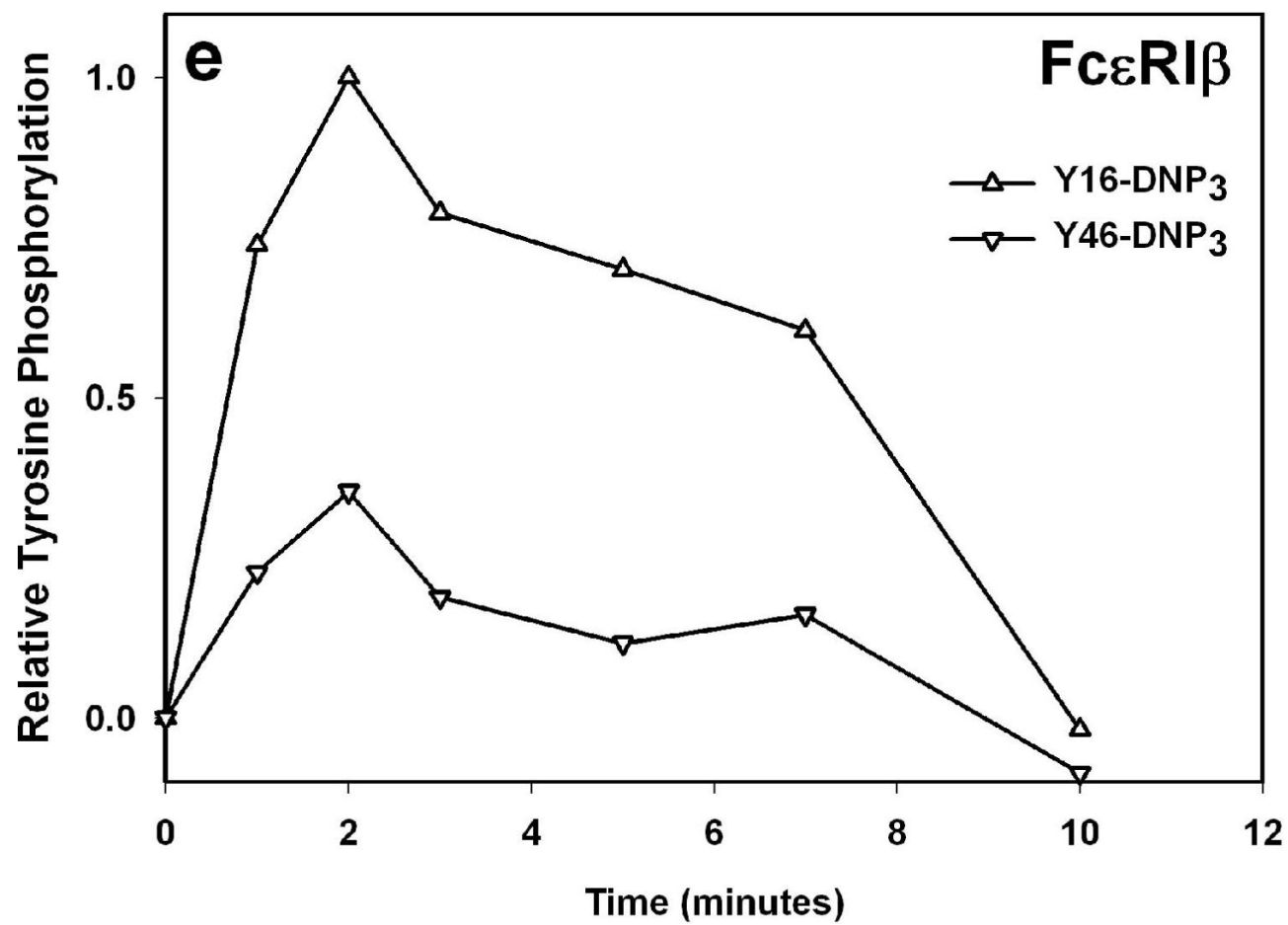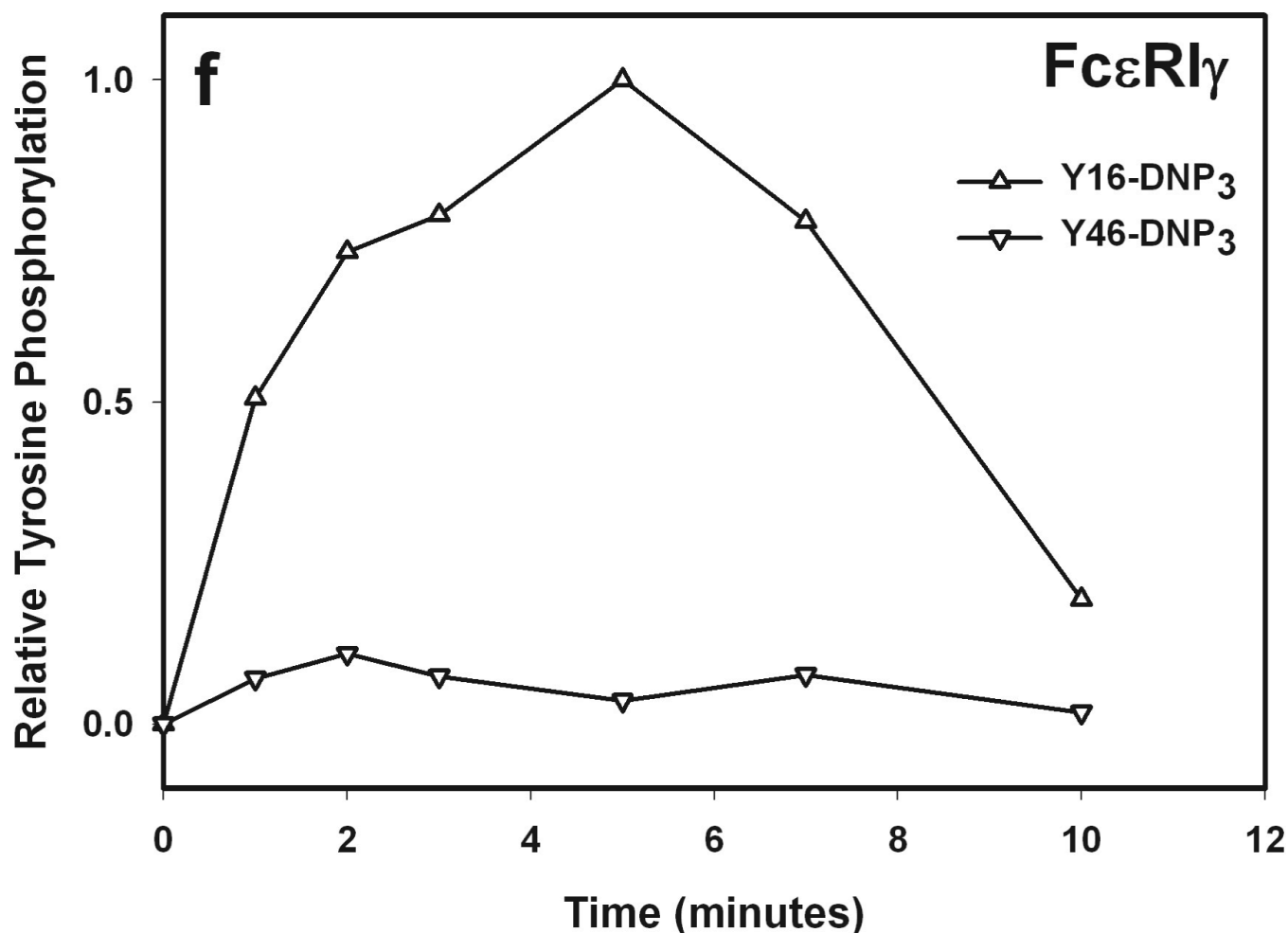
Figure 3. Yn-DNP$_3$-stimulated tyrosine phosphorylation of FcεRI subunits and LAT in RBL mast cells
a) Representative western blot shows tyrosine phosphorylated bands for β and γ$_2$ subunits of FcεRI and LAT for cells treated with buffer only (unstimulated), Y16-DNP$_3$, Y26-DNP$_3$, Y36-DNP$_3$ or Y46-DNP$_3$. Suspended, IgE-sensitized RBL cells were incubated with Yn-DNP$_3$ ligands (30 nM) for 3 min at 37°C, lysed and immunoprecipitated with anti-IgE or anti-LAT on protein A Sepharose beads. Equal cell equivalents of solubilized proteins were boiled with SDS sample buffer, electrophoresed on 12% acrylamide gels, and analyzed by blotting with anti-phosphotyrosine (4G10). b-d) Data from blots were quantified and averaged from 4 independent experiments for Yn-DNP$_3$ mediated tyrosine phosphorylation of FcεRI-β (b), FcεRI-γ$_2$ (c) and LAT (d). Values were normalized with respect to stimulation by Y16-DNP$_3$ for equal cell equivalents. Bars represent standard errors for the 4 experiments. e and f) Time courses for tyrosine phosphorylation of FcεRI-β (e) and FcεRI-γ$_2$ (f) stimulated by Y16-DNP$_3$ (upper curve) and Y46-DNP$_3$ (lower curve).
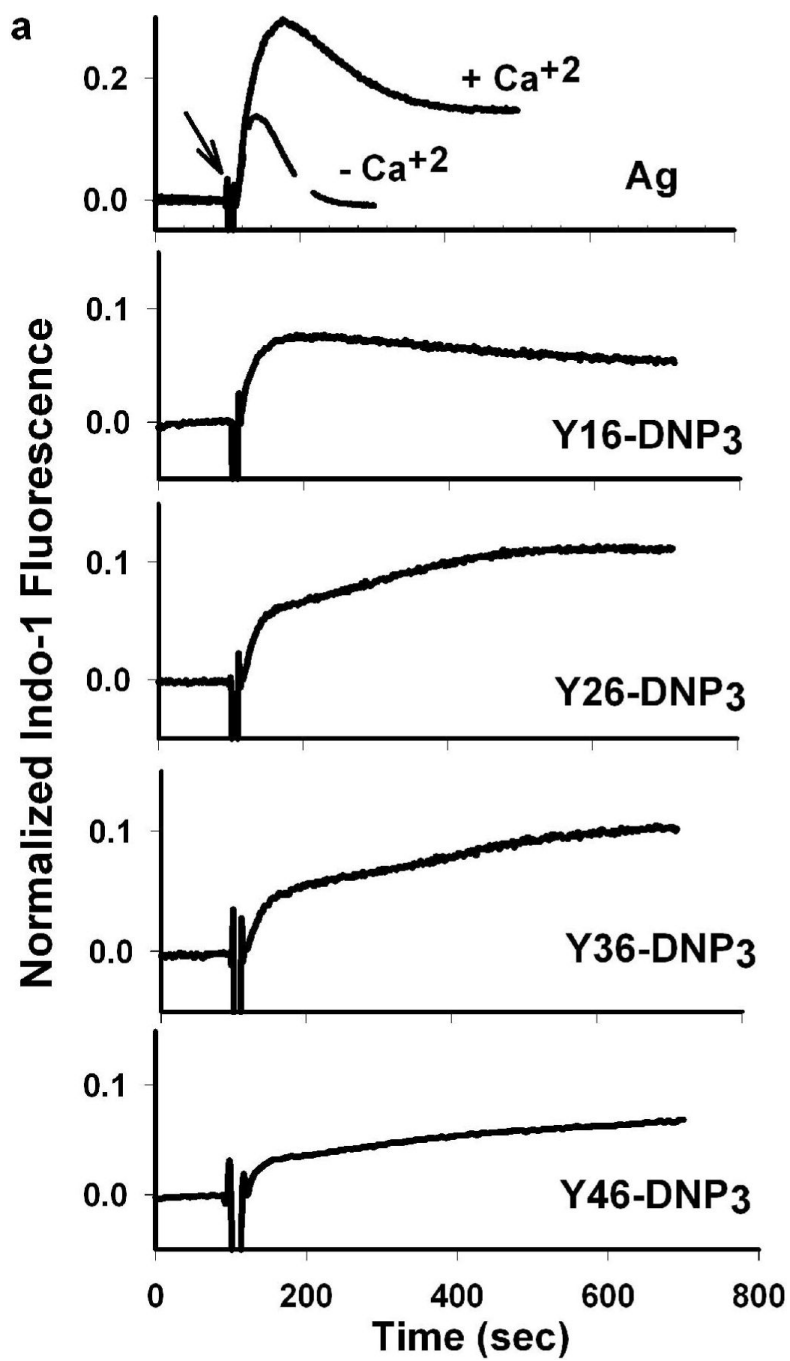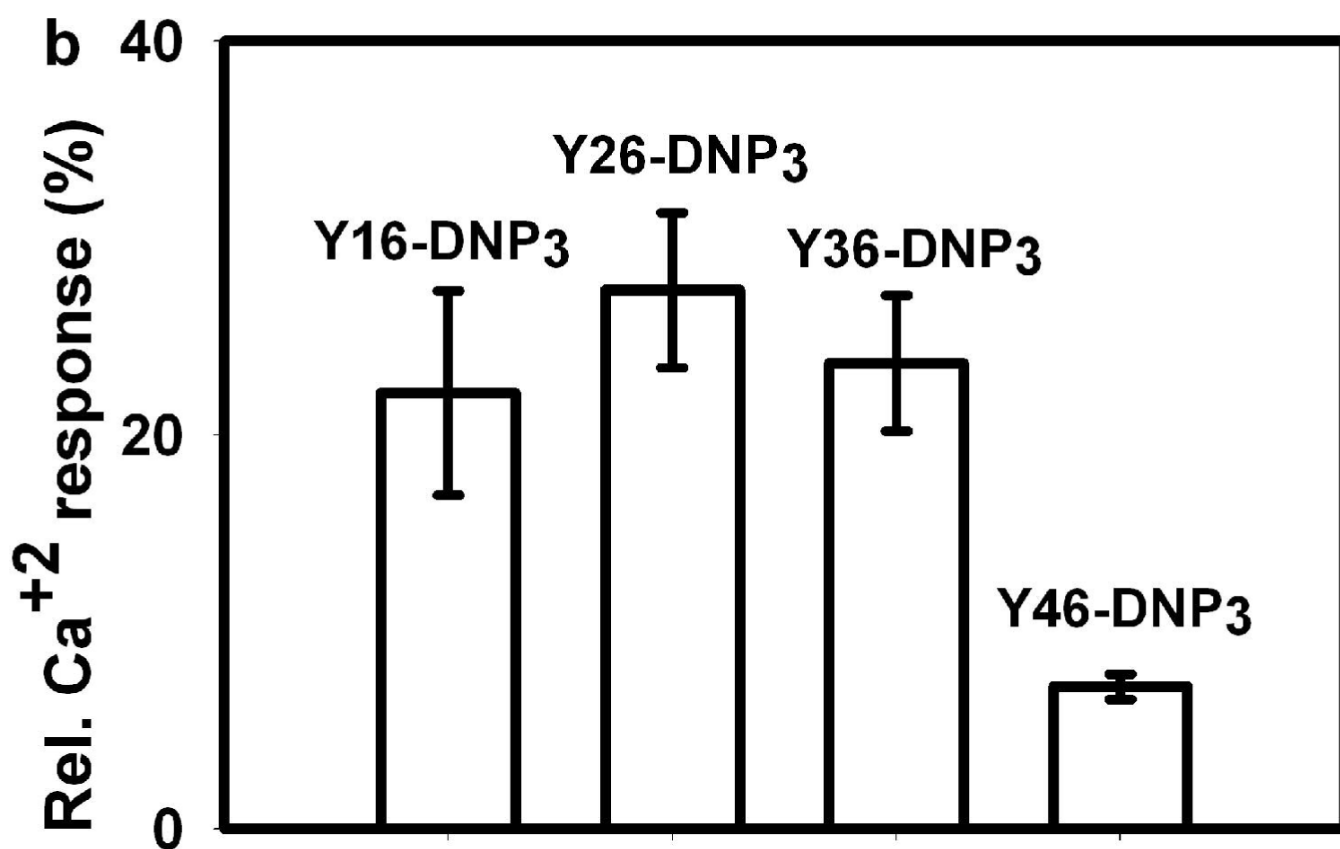
**Figure 4. Ca^{2+} mobilization stimulated by Yn-DNP$_3$ ligands**
a) Representative Ca^{2+} responses of RBL mast cells as stimulated by DNP-BSA (1 μg/ml) or the Yn-DNP$_3$ ligands (30 nM) as specified on individual plots. The baseline was set to 0.0, and ligand addition at 100s is indicated by the arrow. Cells were suspended in BSS including 1.8 mM Ca^{2+} except the designated plot for DNP-BSA (top panel) for which Ca^{2+} was omitted from the buffer. b) Ca^{2+} mobilization integrated for 600 sec after ligand addition, and averaged for each Yn-DNP$_3$ from 5−7 independent experiments. and expressed relative to integrated response to 1μg/μl DNP-BSA. Error bars represent standard errors.
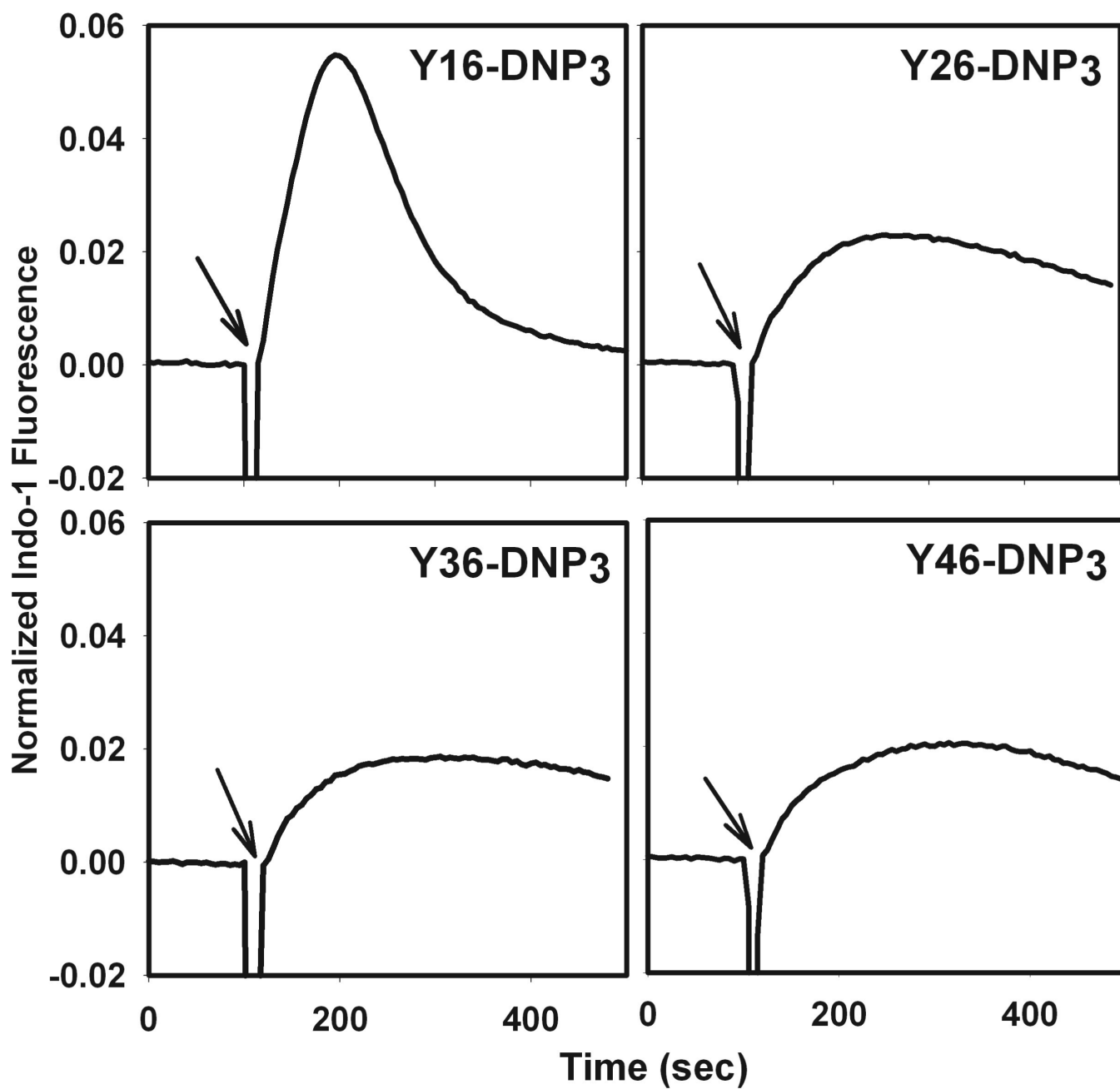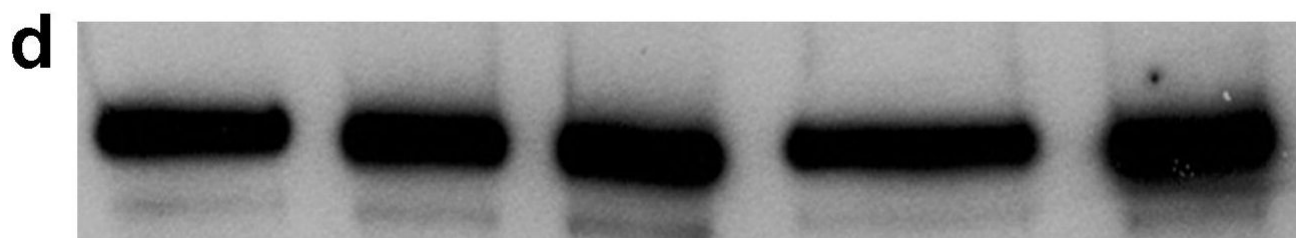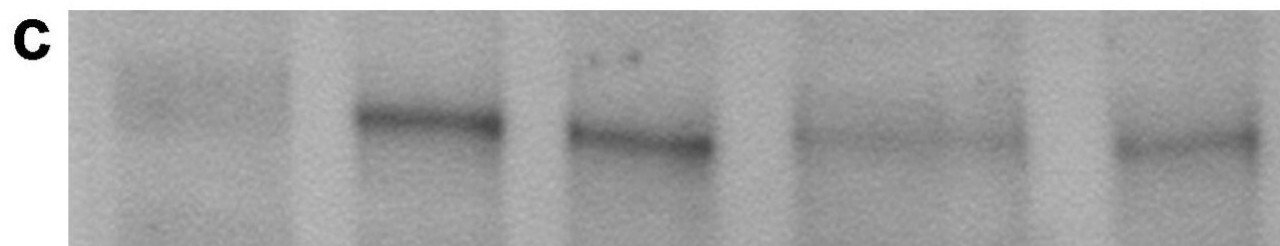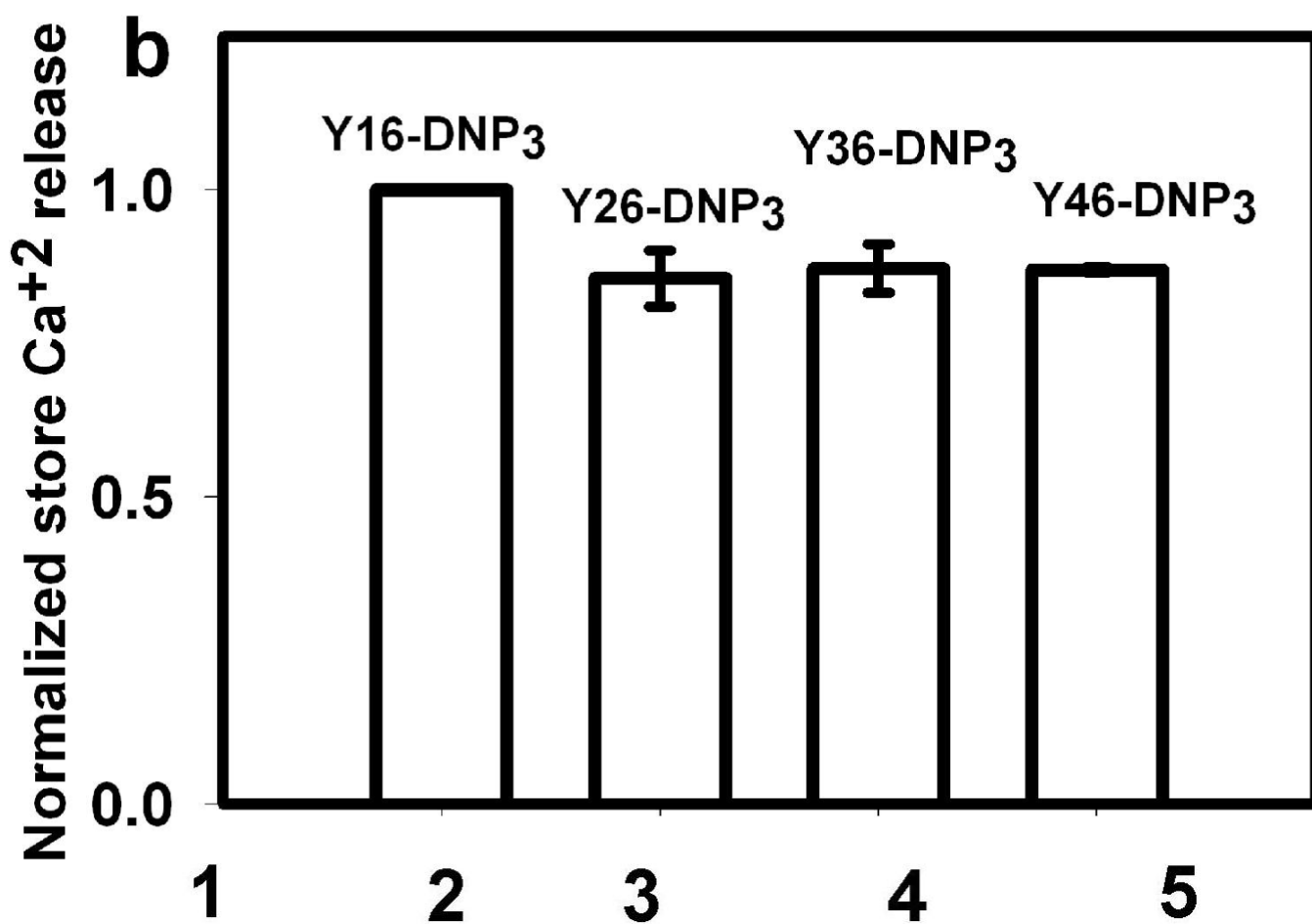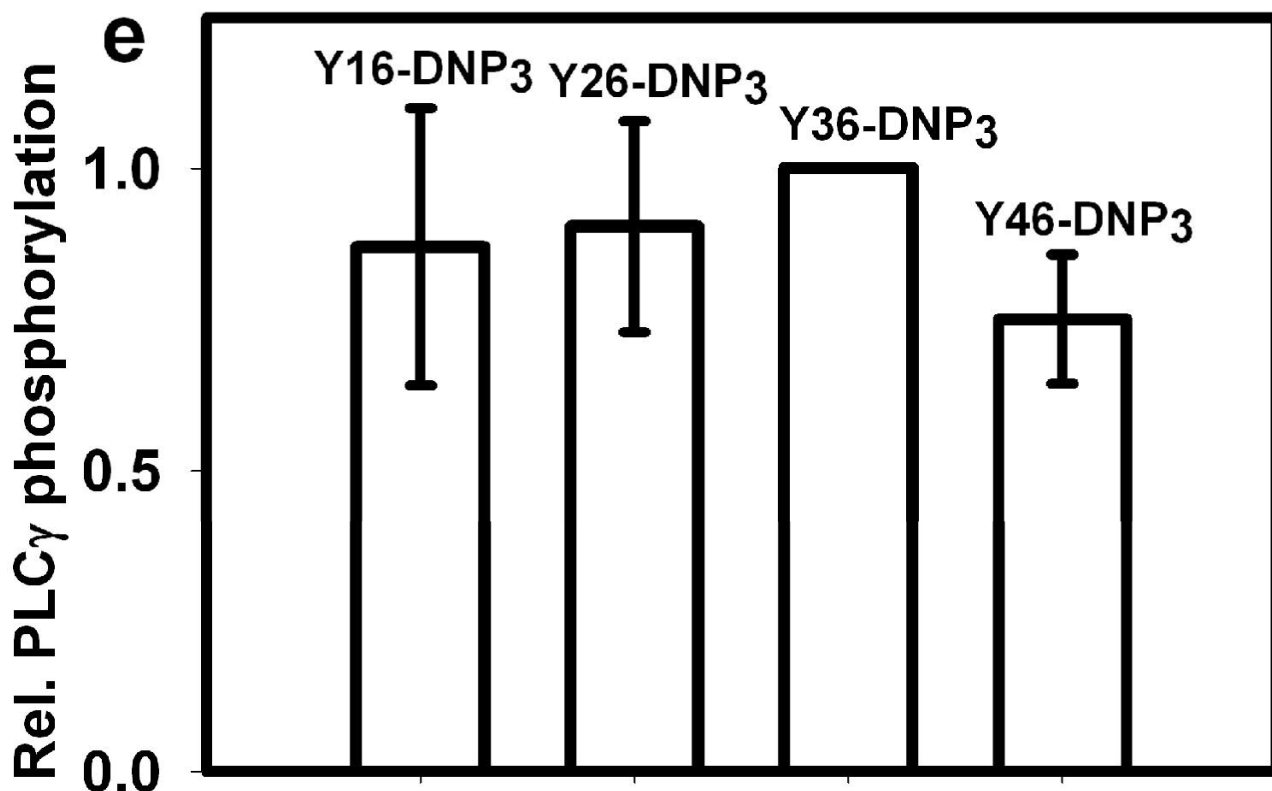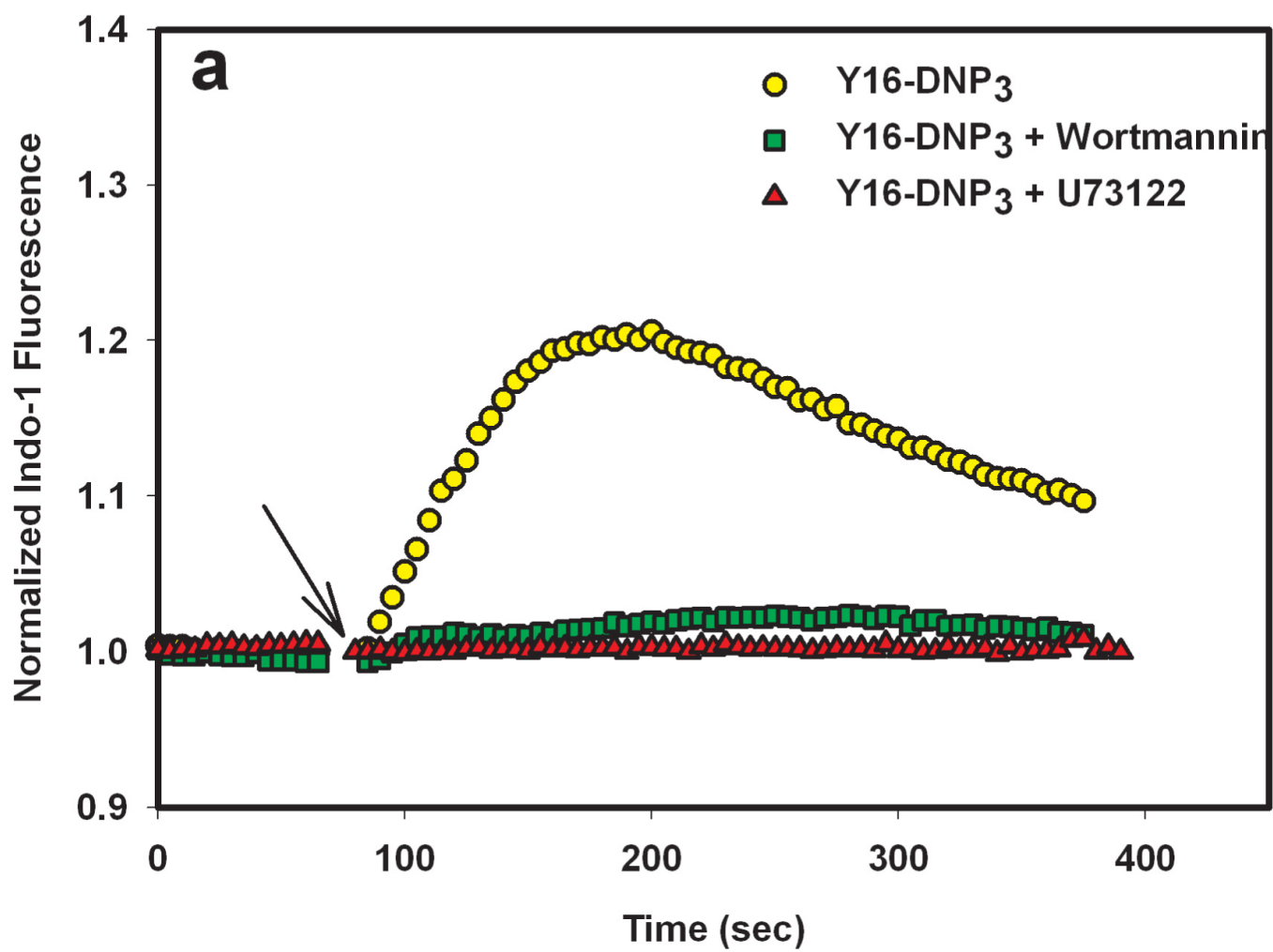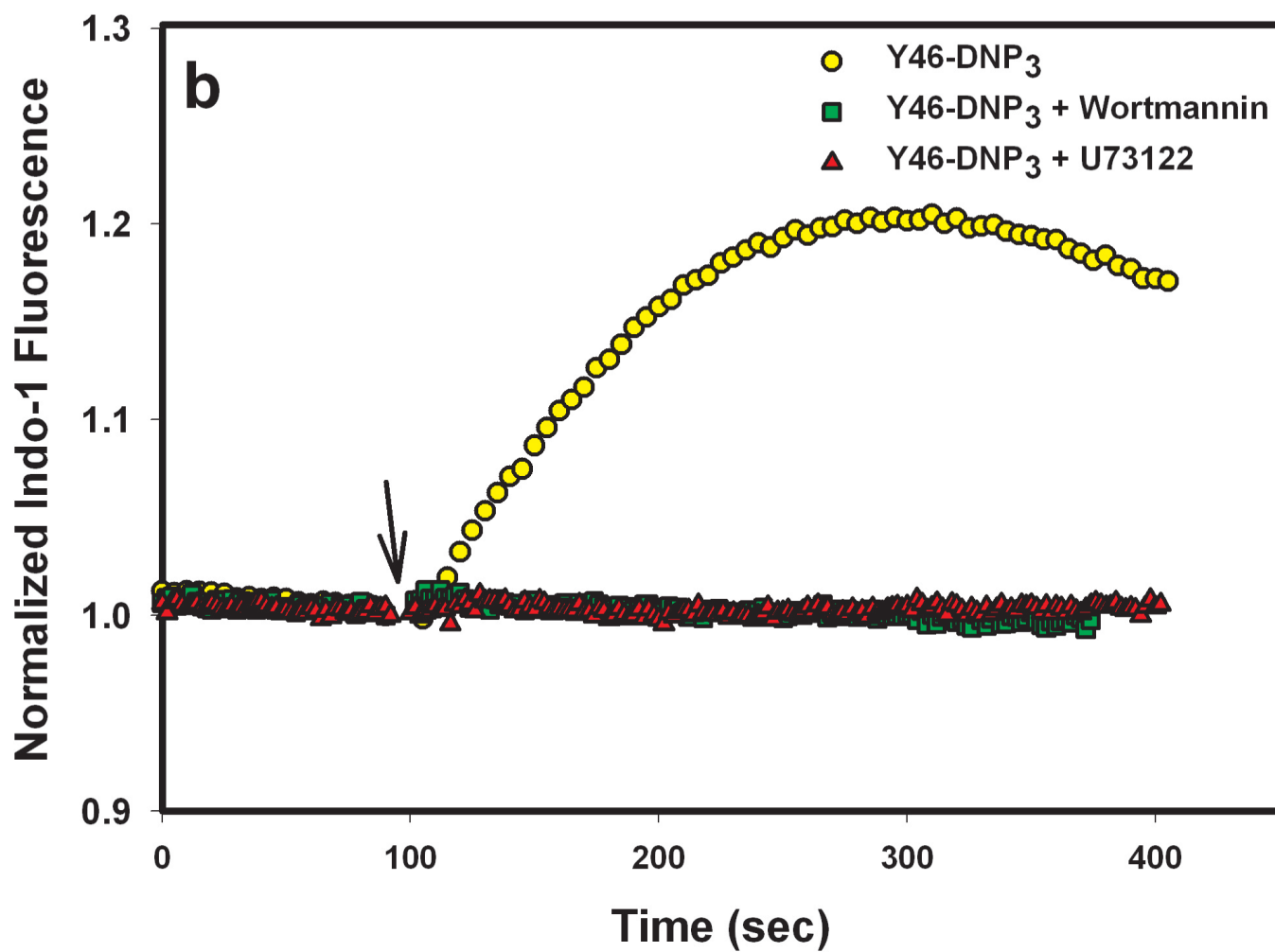
Figure 5. Ca^{2+} release from intracellular stores and tyrosine phosphorylation of PLCγ1 as stimulated by Yn-DNP$_3$ ligands

a) Representative intracellular store release of Ca^{2+} in response to stimulation by the Yn-DNP$_3$ ligands (30 nM) as specified on individual plots. The baseline was set at 1.0, and ligand additions are indicated by arrows. Cells were suspended in BSS except that Ca^{2+} was omitted from the buffer. b) Ca^{2+} release integrated for 300 sec after ligand addition and averaged for each Yn-DNP$_3$ from 3 independent experiments. Values were normalized with respect to stimulation by Y16-DNP$_3$ for equal cell equivalents. Error bars represent standard errors. c) Representative Western blot shows tyrosine phosphorylation of PLCγ1 stimulated with the Yn-DNP$_3$ ligands (buffer (1), Y16-DNP$_3$(2), Y26-DNP$_3$(3), Y36-DNP$_3$(4), Y46-DNP$_3$(5)) and detected with anti-phosphotyrosine (4G10). d) The same blot was stripped and reprobed with anti-PLCγ1 to evaluate sample loading. e) Data from blots were quantified and averaged from 4 independent experiments for Yn-DNP$_3$ mediated tyrosine phosphorylation of PLCγ1. Values were normalized with respect to stimulation by Y36-DNP$_3$ for equal cell equivalents. Bars represent standard errors for the 4 experiments.
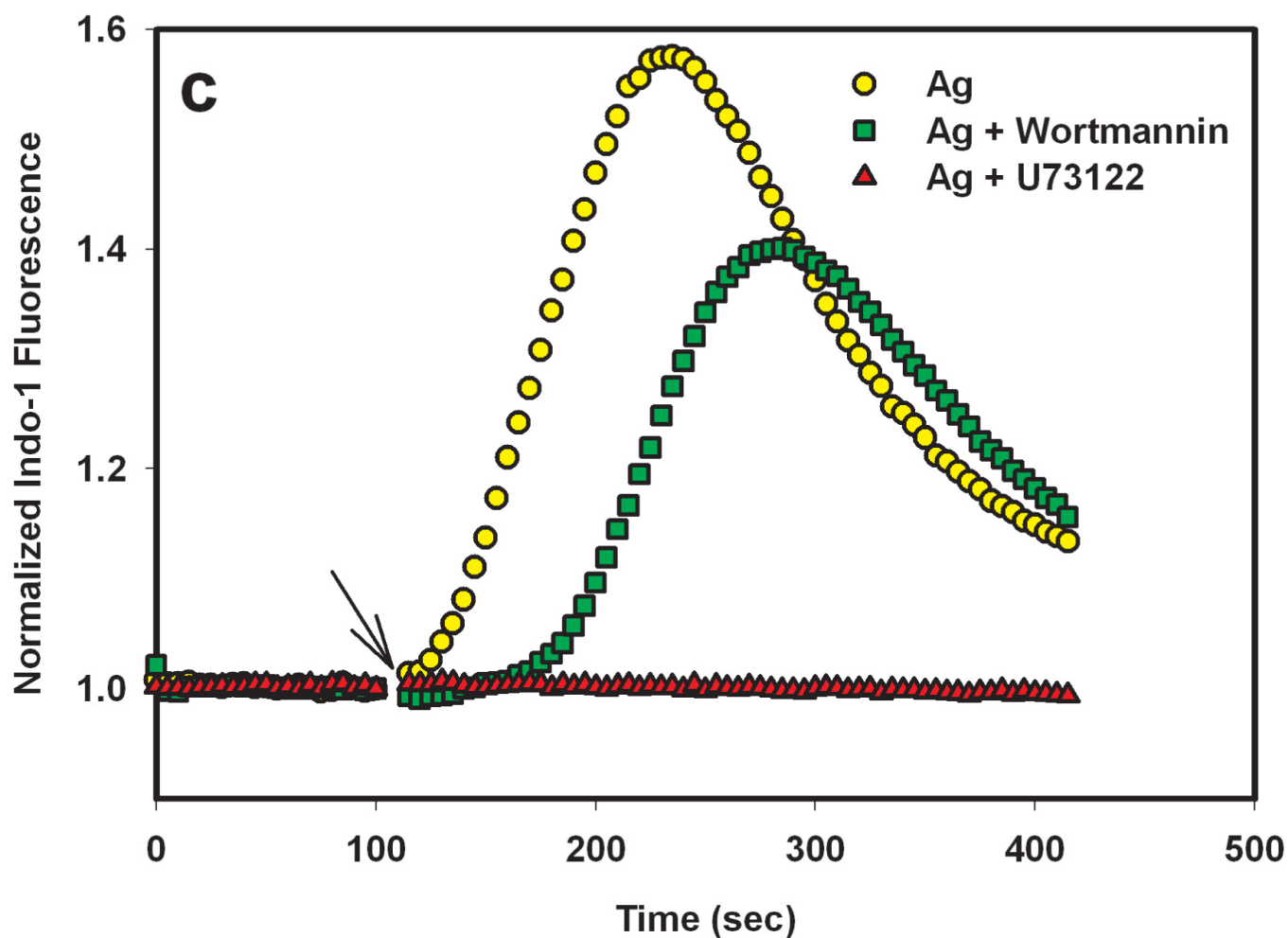
Figure 6.
Effects the PLC inhibitor, U73122, and the PI3 kinase inhibitor, wortmannin, on ligand-stimulated release of Ca^{2+} from intracellular stores. Cells were pre-incubated for 5 min in the absence or presence of either 1 μM U73122 or 200 nM wortmannin prior to addition of Y16-DNP3 (a), Y46-DNP (b), or 1 μg/mL DNP-BSA (c) as in Fig. 5.

Table 1

Physical properties of Yn-DNP$_3$ ligands depicted in Figure 1a

Name[a]	L (nm)[b]	D (nm)[c]	K$_d$ (sol; nM)[d]	K$_d$ (cell; nM)[e]
Y16-DNP$_3$	2.7	5.2 (±0.9)	3.0 ± 1.0	1.5 ± 0.5
Y26-DNP$_3$	4.4	6.9(±1.3)	4.0 ± 1.0	1.2 ± 1.0
Y36-DNP$_3$	6.1	10.4(±1.6)	4.0 ± 1.0	1.5 ± 1.0
Y46-DNP$_3$	7.8	13.1(±2.5)	4.0 ± 1.0	1.6 ± 0.5

[a] Y-shaped, trivalent (DNP$_3$) ligand with n (= 16, 26, 36, or 46) bases in each of three single DNA strands that are annealed into the double stranded structure. Sequences of respective single strands are shown in Supplemental Table S1.

[b] Estimated length (L) of each double-stranded arm of respective Yn-DNP$_3$, based on length per base pair (0.34 nm).

[c] Average rigid distances (D) between 5′ termini of Yn scaffolds for Yn-DNP$_3$ ligands as determined by fluorescence resonance energy transfer measurements; numbers in parentheses indicate the range of distances between different termini due to some aplanarity and asymmetry in the rigid scaffolds (JB Lee, D Luo, in preparation).

[d] Apparent dissociation constant for Yn-DNP$_3$ ligands binding to IgE in solution, averaged from three experiments for each ligand (± standard deviation).

[e] Apparent dissociation constant for Yn-DNP$_3$ ligands binding to IgE-FcεRI on RBL cells, averaged from three experiments for each ligand (± standard deviation).